Dissertação de Mestrado

Inatel
Instituto Nacional de Telecomunicações

A Graphene-Based Polarization-Insensitive Amplitude and Phase Electro-Optical Modulator.

BRAIAN NATHAN DE OLIVEIRA ANDRADE

MAY / 2022

A GRAPHENE-BASED POLARIZATION-INSENSITIVE AMPLITUDE AND PHASE ELECTRO-OPTICAL MODULATOR.

BRAIAN NATHAN DE OLIVEIRA ANDRADE

Dissertação apresentada ao Instituto Nacional de Telecomunicações, como parte dos requisitos para obtenção do Título de Mestre em Telecomunicações.

ORIENTADOR: Prof. Dr. Jorge Ricardo Mejía-Salazar.

COORIENTADOR: Prof. Dr. Felipe Beltrán-Mejía.

Santa Rita do Sapucaí
2022

Andrade, Braian Nathan de Oliveira
A553a
A graphene-based polarization-insensitive amplitude and phase electro-optical modulator./ Braian Nathan de Oliveira Andrade. – Santa Rita do Sapucaí, 2022.
86 p.

Orientador: Prof. Dr. Jorge Ricardo Mejía-Salazar / Prof. Dr. Felipe Beltrán-Mejía.
Dissertação de Mestrado em Telecomunicações – Instituto Nacional de Telecomunicações – INATEL.
Inclui bibliografia.

1. Grafeno 2. Insensibilidade a polarização 3. Modulação em amplitude e fase 4. Modulador eletroóptico 5. Amplitude and Phase Modulation 6. Mestrado em Telecomunicações. I. Mejía-Salazar, Jorge Ricardo. II. Beltrán-Mejía, Felipe III. Instituto Nacional de Telecomunicações – INATEL. IV. Título.

CDU 621.39

Ficha Catalográfica elaborada pelo Bibliotecário da Instituição
CRB6-2718 – Paulo Eduardo de Almeida

FOLHA DE APROVAÇÃO

Dissertação defendida e aprovada em _____/_____/_____, pela comissão julgadora:

Prof. Jorge Ricardo Mejía Salazar
INATEL

Prof. Dr. Danilo Henrique Spadoti
UNIFEI

Prof. Dr. Ramon Maia Borges
INATEL

Coordenador do Curso de Mestrado
Prof. Dr. José Marcos Camara Brito

”Human progress has always been driven by a sense of adventure and unconventional thinking.”

Dr. Andre Geim, awarded 2010 Nobel Prize in Physics ”for groundbreaking experiments regarding the 2D material graphene.”

Dedico esta dissertação aos meus pais
Antônio Carlos A. Andrade (in memoriam)
e Alda Marta de O. Andrade,
que me ensinaram o valor da educação.

Agradecimentos

Depois de longos e desafiadores anos de estudo, não posso deixar de agradecer a todos que tornaram a conclusão deste trabalho possível. Agradeço a minha família pelo apoio incondicional, a minha namorada Ana Cristina por estar ao meu lado mesmo nos momentos mais difíceis, ao meu amigo de quatro patas Gollum que me ajudou mais do que é possível expressar, aos diversos amigos de laboratório sempre dispostos a tomar um cafezinho, aos amigos do cotidiano que me incentivaram a superar grandes obstáculos, a sorte de ter tido dois grandes orientadores Felipe B. Mejía e Jorge R. Mejía-Salazar pelos inestimáveis ensinamentos, e a instituição INATEL e seus colaboradores pelo alto nível de qualidade, zelo, dedicação e profissionalismo.

Braian Nathan de Oliveira Andrade

Summary

List of Figures

List of Tables

List of Abbreviations and Acronyms

2D	Bidimensional
5G	Fifth-generation mobile communication network
6G	Sixth-generation mobile communication network
AZO	Aluminium-doped Zinc Oxide
CMOS	Complementary Metal-Oxide-Semiconductor
CVD	Chemical Vapor Deposition
EBL	Electron Beam Lithography
FEM	Finite Element Method
Gb/s	Giga bits per second
GHz	Giga Hertz
GZO	Gallium-doped Zinc Oxide
IoT	Internet of Things
ITO	Indium Tin Oxide
M-PAM	Multilevel Pulse Amplitude Modulation
M-PSK	Multilevel Phase Shift Keying
M-QAM	Multilevel Quadrature Amplitude Modulation
Mb/s	Mega bits per second
MD	Modulation Depth
MHz	Mega Hertz
MZM	Mach-Zehnder modulator
NRZ	Non Return to Zero
PIC	Photonic Integrated Circuits
PML	Perfectly Matched Layer
SOI	Silicon-On-Insulator
Tb/s	Tera bits per second
TE	Transverse Electric
THz	Tera Hertz
TM	Transverse Magnetic
WDM	Wavelength Division Multiplexing

List of Symbols

α	Absorption
α_{TE}	Absorption of TE mode
α_{TM}	Absorption of TM mode
$\Delta\phi$	Phase change
Δn_{eff}	Variation of the effective refractive index
$\Delta n_{\text{eff}}^{TE}$	Variation of the effective refractive index of TE mode
$\Delta n_{\text{eff}}^{TM}$	Variation of the effective refractive index of TM mode
ΔV	Voltage required by the modulator
η	Graphene's carrier density (or graphene's doping level)
Γ	Dispersion rate
$\hbar$	Planck's constant divided by 2π
λ	Wavelength
μ	Graphene's carrier mobility
ν	Photon's frequency
ω	Angular frequency
Ω	Electrical resistance
σ_{inter}	Inter-band conductivity
σ_{intra}	Intra-band conductivity
$\sigma_{\|\|}$	Graphene's conductivity
τ	Electron relaxation time
ε_0	Free space permittivity
ε_{r}	Relative permittivity
$\varepsilon_{\perp}$	Out-of-plane permittivity
$\varepsilon_{\|\|}$	In-plane permittivity
A_{gra}	Total area of graphene
Au	Gold
C	Capacitance
CH_4	Methane
CO_2	Carbon dioxide
Cu	Copper
d	Thickness of the dielectric layer below the graphene
d_g	Thickness of graphene's layer
E	Energy
e	Electron charge
E_f	Fermi energy (also called chemical potential)
E_{bit}	Energy per bit

eV	Electron volts
$f(E)$	Fermi Dirac distribution function
$f_{3\,\mathrm{dB}}$	3dB modulation speed parameter
$GaAs$	Gallium Arsenide
Ge	Germanium
h	Waveguide's height
H_2	Hydrogen
HfO_2	Hafnium Dioxide
InP	Indium Phosphide
k_{B}	Boltzmann constant
L	Modulator's length
$LiNbO_3$	Lithium Niobate
n_{eff}	Effective refractive index
n_{HfO_2}	Effective refractive index of HfO_2
n_{SiO_2}	Effective refractive index of silica
n_{Si}	Effective refractive index of silicon
Ni	Nickel
R	Total resistance of the device
R_{c}	Electrode contact resistance
R_{s}	Graphene sheet resistance
Si	Silicon
SiC	Silicon Carbide
SiN	Silicon Nitride
SiO_2	Silica
T	Room temperature
t_{slab}	Slab thickness
V	Applied voltage
V_0	Graphene's natural offset
V_{f}	Fermi Velocity
w	Waveguide width
w_{g}	Effective width of graphene

Resumo

Modulador Eletro-Óptico de Fase e Amplitude
Insensível à Polarização Baseado em Grafeno

Braian N. O. Andrade

Dissertação de Mestrado
Inatel - Instituto Nacional de Telecomunicações
Santa Rita do Sapucaí - MG - Brasil - 2021

Esta dissertação relata o projeto de um modulador eletro-óptico baseado em grafeno, capaz de modular em amplitude e fase, com insensibilidade à polarização e estrutura compacta. O projeto consiste de uma camada única de grafeno depositada sobre um guia de onda de silício com um espaçador dielétrico fino de dióxido de háfnio. As dimensões foram ajustadas buscando alcançar a insensibilidade à polarização e maximizar a interação luz-grafeno, otimizando o desempenho. Os resultados indicam modulação insensível à polarização em amplitude e fase com consumo de energia inferior a 1 pJ/bit e largura de banda de 3dB de $11,57$ GHz, capaz de operar de 1250 nm à 1700 nm abrangendo todos os comprimentos de onda utilizados em comunicações ópticas ($1260-1625$ nm). O dispositivo foi projetado considerando materiais e geometrias de fácil implementação, compatíveis com os processos atuais de fabricação. Este conceito pode auxiliar no desenvolvimento de novas tecnologias de telecomunicações como *hardwares* fotônicos integrados, interconexões ópticas, microchips ópticos, etc. ajudando a lidar com a crescente demanda por comunicações e o tráfego de informações.

***Palavras-Chave*:** Grafeno; Insensibilidade à polarização; Modulação em amplitude e fase; Modulador eletroóptico

Abstract

Graphene-Based Polarization-Insensitive Amplitude and Phase Electro-Optical Modulator

Braian N. O. Andrade

Masters Dissertation
Inatel - Instituto Nacional de Telecomunicações
Santa Rita do Sapucaí - MG - Brazil - 2021

This dissertation reports the design of a graphene-based electro-optical modulator, capable of modulating in amplitude and phase, with polarization insensitivity, and compact structure. The design consists of a graphene single layer deposited onto a silicon waveguide with a thin hafnium dioxide dielectric spacer. The dimensions were adjusted to achieve polarization insensitivity and maximize light-graphene interaction while optimizing performance. The results indicate a modulation insensitive to polarization for amplitude and phase operation with energy consumption less than 1 pJ/bit and a 3dB-bandwidth of 11.57 GHz, capable of operating from 1250 nm to 1700 nm covering all wavelengths used in optical communications ($1260 - 1650$ nm). The device was designed considering easily implementable materials and geometries that are compatible with current manufacturing processes. This concept can assist in the development of future telecommunication technologies such as integrated photonic hardware, optical interconnects, optical microchips, etc. helping to cope with the ever-growing demand for improved communication and information traffic.

***Key words*:** Amplitude and Phase Modulation; Electro-optical Modulator; Graphene; Polarization Insensitivity.

Chapter 1

Introduction

1.1 Contextualization

THE seamless integration of wireless THz links with fiber-optics infrastructure and microelectronic devices is crucially important for the successful development of future 6G (sixth-generation mobile communication networks) technology, envisaging data rates in the order of hundreds of Gb/s per link [1, 2]. This convergence of wireless THz signals with fiber optics and electronics, mediated by photonics, has stimulated research in various directions, such as in the THz-to-optical (optical-to-THz) conversion at the wireless receiver (transmitter) using modulators (photodiodes) [3–6]. Indeed, plasmonic modulators were recently used for direct THz-to-optical conversion at the THz receiver [5], avoiding complex all-electronic up/down-conversion mechanisms [7]. On the other hand, at the chip-scale, optical and electronic (optoelectronic) signals must also be seamlessly integrated to prevent communication performance bottlenecks. In particular, the main drawbacks of conventional electronic interconnects (for instance, copper cables), associated with inherent losses, dispersion, and crosstalk, must be overcome to avoid their increasingly noticeable detrimental effects as the number of intra- and inter-chip data connections increases exponentially year after year [8, 9].

Optical interconnects, on the contrary, offer intrinsic advantages like, for example, reduced levels of losses and fabrication costs, motivating intense research activity during the last decades with the aim to provide a way to integrate photonics with state-of-the-art nanoelectronics [10]. Particular interest has been given to the design and development of optical modulators, the workhorse of these interconnects. The key driving force behind optical modulators stems from the ability to dynamically tune the light properties, through the control of the material properties, to convert external electrical signals into high-bit rate light signals [11]. Since different material properties can be used

for optical modulation, optical modulators are commonly classified according to the physical principle on which they are based, as will be discussed in Chapter 2.

1.2 Historical Background

Optical modulators are at the core of fiber-optic systems, from metropolitan to long-haul terrestrial and undersea optical communications infrastructures [12]. These devices evolved, thanks to sustained innovations in integrated electronics, from the first bulky electro-optical modulator (produced in the sixties to modulate the output of gas lasers [13]) to highly integrated modern photonic circuits [10]. The first step towards integration came with the advent of semiconductor laser diodes, which replaced large gas lasers [14,15]. The latter approach uses the semiconductor driving current to directly modulate the output power of a semiconductor laser [16], thus being called direct modulation. The variable electrical current (electrical input data signal) interferes with the population of electrons and, consequently, with the processes of spontaneous/stimulated emission of the laser, enabling modulation of the output laser power [17, 18]. The simplicity and low cost of direct modulation, as well as the integration of the source and modulator in a single device, made this approach advantageous for several years [19]. In fact, its first implementations reached 90 Mb/s through direct modulation and multimode fibers [20]. Despite the advantages of direct modulation, fundamental problems associated with frequency chirp and wavelength excursion began to become apparent with technological advances and the need for higher bit rates [12, 21].

The exploitation of the light propagation properties in dielectric materials to develop external optical modulators, based on waveguide modulators, emerged as an alternative to overcome the limitations associated with direct optical modulation [22, 23]. Importantly, these waveguides harness the complementary physics between electronic and photonic technologies to provide high-performance integrated solutions. In particular, the linear electro-optic effect, also known as the Pockels-effect, is the concept behind most of the high-speed modulators of present-day to impress information from electrical signals onto photonic waveguides [24]. This process is carried out through the change induced by the electrical signal on the real and imaginary part of the refractive index of the waveguide medium, labeled, respectively, as the electro-refraction and electro-absorption mechanisms. Due to its high electro-optical coefficient (31 pm/V), the lithium niobate material has led the commercially available modulators since its first implementation in the 1980s [12]. However, drawbacks associated with the low refractive index contrast, yielding weak optical confinement, hamper the further integrability of lithium niobate-based waveguides. These limitations become predominantly

important when we are trying to increase devices data rates from Gb/s to Tb/s, where photonic-electronic integration is essential to reduce both the system-level power consumption and the device-level capacitance of connecting the transmitter modulators as well as the receiver photodetectors [25].

The dominance of silicon (Si) in the microelectronics industry prompted researchers to investigate silicon photonics during the last decades, to overcome limitations from lithium niobate approaches, mainly motivated by the possibility of direct integration with electronics (through CMOS packaging techniques) in a cost-effective manner [26]. Indeed, nowadays achievements include integrated high-speed silicon optical transceivers operating at tens of gigabits per second, arranged on a single optical bus, to address the demand for high-bandwidth optical interconnects [10].

1.3 Current Scenario and Future Perspectives

Currently, the rampant growth in the demand for data traffic puts pressure on long-distance transport networks. According to Cisco's Annual Internet Report [1], in 2020 the global data traffic was greater than 10^{21} bytes (zettabyte), and by 2023 more than 27 billion devices are expected to be connected. Changes in consumer habits, mainly due to the COVID-19 pandemic, have increased Internet consumption for remote work and learning, resulting in an increase of up to 100% in the residential network and $10 - 20\%$ in mobile traffic [2]. With the development of new mobile communications technologies such as 5G and 6G, and applications such as the Internet of Things (IoT), real-time streaming, cloud processing, augmented reality, etc., tend to further increase the amount of data over the optical networks [27]. In this sense, scientists are forced to think ahead and predict the behavior of traffic and the impact of these innovations on the system. For this reason, research on network devices is still very active today.

Unfortunately, today's electronic circuits are approaching physical limits in terms of speed and data transmission rate [28]. Intrinsic problems such as Ohmic losses, parasitic capacitances, interference, limited speed, heating, high power consumption, size, impedance, etc., have become difficult to circumvent [29]. The most promising proposals to overcome the limitations of electronic circuits are related to optics [30]. Inspired by electronic semiconductor technologies such as high production capacity and integration into functional and reliable microchips, researchers hope that silicon-based optical devices will follow a similar path [31]. The production of integrated optical components is studied since the first optical systems, but gained new impulses with the development of silicon photonics [32].

The silicon photonics has been an effervescent research topic for many years [12,32], mainly after the advances in lithography processes that made it possible to produce small waveguides with high precision (< 10 nm), and low losses (< 1 dB/cm), which can be bent with curves of radius less than $10\,\mu$m, allowing the creation of integrated, complex, and compact optoelectronic circuits [32]. In addition to being used extensively in electronics, silicon also serves as a gateway to optics [33,34]. However, it is a material with a low electro-optical coefficient, making it difficult to change its refractive index, resulting in optical modulators with typical lengths of 3 mm to 11 mm [35], too large in terms of Si-photonics, and impractical for use inside optical-chips [36]. Therefore, optical modulation has to be done in other ways, an alternative is modulators based on carrier density effects [12], but these devices can be speed limited due to carrier lifetime, which is typically $1 - 10$ ns [12, 36]. Other approaches exploit the tiny dimensions of Si waveguides in microring resonant modulators, achieving high modulation speed ($10 - 25$ GHz) [37–39], having some of the best energy consumption per bit ratio [40], but the operating band is intrinsically narrow (few nanometers around the resonance wavelength), also the device is highly sensitive to the variation of temperature [41–43]. More complex modulating structures are possible, but sophisticated design and stringent manufacturing requirements limit their applications.

To compensate for the low electro-optical coefficient of silicon waveguides, researchers have exploited hybrid designs with other dielectric materials. Particular emphasis has been given to Indium Tin Oxide (ITO), Aluminum-doped Zinc Oxide (AZO), and Gallium-doped Zinc Oxide (GZO) [44–46], which in addition to being low-loss transparent conductive films, are compatible with Complementary Metal-Oxide-Semiconductors (CMOS) and, therefore, easily integrable with silicon [47]. On the other hand, the new physical properties of recently discovered two-dimensional (2D) materials have been shown promising to develop the next generation of optoelectronic devices [48–53]. Among the 2D materials, graphene has drawn special attention for its exceptional electronic and photonic characteristics [54], such as strong coupling with light [55], high operating speed [56], high carrier mobility at room temperature [57], large absorption capacity over a wide spectrum [58, 59], variable optical conductivity [60], and compatibility with CMOS [61]. These properties make graphene an optimal material for studies in nanoelectronics [52, 62], photonics [63], optoelectronics [64, 65], plasmonics [66–68], and metamaterials [51, 69]. When integrated with silicon waveguides, graphene can be used as an active medium for optical modulators [70], presenting excellent results such as high modulation speed and wide bandwidth, in addition to the small scale and low loss [70, 71], which is essential for on-chip optical interconnections. Up to date, several theoretical and experimental

proposals for graphene-based optical modulators have been demonstrated [57, 72–75].

1.4 Graphene Modulators

The first optical modulator using graphene was presented by Liu et al. in 2011 [70]. The modulator consisted of a single layer of graphene over a rectangular waveguide of doped silicon. Experimentally achieved a modulation depth of 0.1 dB/μm, capable of operating with the wavelength from 1350 nm to 1600 nm, and 3dB-bandwidth of 1 GHz. This result is comparable to those of commercially used semiconductor modulators. Later, the same group experimentally demonstrated a modulator with two layers of graphene over a rectangular waveguide, reaching a modulation depth of 0.16 dB/μm [71]. For comparison, this modulation depth per unit of length is 320 times greater than a typical Mach-Zehnder modulator [12, 36], which proves the feasibility of this type of device. Since then, several proposals for optical modulators based on graphene-silicon have been presented.

In 2014, M. Mohsin et al. [76] experimentally demonstrated an amplitude modulator using two layers of graphene, achieving 0.06 dB/μm, and 3dB-bandwidth of 670 MHz. A. Phatak et al. in 2016 [77] numerically presented a graphene-silicon modulator with a slot-type waveguide, reaching a modulation depth of 0.144 dB/μm; In the same year, Y.T. Hu et al. [78] proposed and experimentally demonstrated, an optical modulator using a rectangular silicon waveguide covered with a single layer of graphene, reaching a modulation depth of 0.15 dB/μm, capable of operating up to 10 Gb/s, with a 3dB-bandwidth of 5.9 GHz; Later the same group reached 20 Gb/s with a similar device [79]. In 2017, M. Fan et al. [80] presented a multi-layer graphene amplitude modulator, reaching a modulation depth of 0.16 dB/μm, with a 3dB-bandwidth of 30.6 GHz; In the same year, M. Shah et al. [81] propose an amplitude modulator with two layers of graphene incorporated with a D-microfiber, with a modulation depth of 0.22 dB/μm, and a 3dB-bandwidth of 97.26 GHz. In 2018, V. Sorianello et al. [82] experimentally demonstrated an MZM (Mach-Zehnder Modulator) with a graphene layer on each arm, achieving a modulation depth of 0.12 dB/μm and 3dB-bandwidth of 5 GHz; In the same year, L. Ji et al. [83] proposed a modulator with two graphene layers over a dual-slot silicon waveguide, reaching a modulation depth of 0.35 dB/μm, capable of operating from 1200 nm to 1900 nm, with a 3dB-bandwidth of 79.6 GHz. In 2019, Z. Yang et al. [84] presented a polarization-insensitive graphene-based modulator with a structure of coupling and conversion of guided modes, reaching a modulation depth of 0.06 dB/μm, capable of operating from 1500 nm to 1600 nm, with a 3dB-bandwidth of 14.3 GHz on a device that is 270 μm long; In the same year, J. Luan et al. [85] propose

a multilayer graphene-based modulator over a hybrid plasmonic waveguide with two slots, achieving a modulation depth of 0.52 dB/μm, with a 3dB-bandwidth of 150 GHz. V. Sorianello et al. [74] in 2020, presented two graphene-silicon-based modulators, with one and two graphene layers, achieving 0.06 dB/μm and 0.12 dB/μm respectively, the authors claim that, with better optimization of contacts, their devices can reach a 3dB-bandwidth of 100 GHz. More recently, in 2021, Y. Ma et al. [86] presented a polarization-insensitive modulator based on a slot-type silicon waveguide, and achieved a modulation depth of 0.37 dB/μm, capable of operating from 1460 nm to 1620 nm, with a 3dB-bandwidth of 50 GHz; And W. Chen et al. [87] presented a polarization-insensitive modulator using two layers of graphene embedded in a silicon nitride (SiN) waveguide, reaching a modulation depth of 0.1 dB/μm, capable of operating from 1100 nm to 1645 nm, with a 3dB-bandwidth of 53 GHz.

The success of graphene-silicon has resulted in a fertile platform for research and development; over time, a wide variety of modulators that use graphene as an active medium, combined with silicon waveguides, have been proposed. The advances and refinements of different techniques made it possible to increase the modulation depth, wavelength range, and operating speed. Currently, this research is still very active, and every year many articles are published proposing the most different designs, using the combination of several other materials, and exploring different physical effects.

1.5 Research Opportunity

The vast majority of the proposals for graphene-based optical modulators presented so far are polarization-sensitive. Polarization-sensitive devices require special mechanisms to control the propagation of light, which limits their applicability [36]. As an example, linearly polarized systems need a polarization controller between the transmitter and the modulator [88, 89], increasing the complexity and costs. Furthermore, for systems with circular or elliptical polarization, it becomes necessary to decompose the light into two orthogonal components before modulation, as it was made in Yang et al. 2019 [84], resulting in an increased level of losses [90]. These drawbacks motivate the search for polarization-insensitive devices for optical communication systems.

Currently, a small portion of the modulators presented is insensitive to polarization, for example Refs. [90–92]. Unfortunately, most proposals often have sophisticated geometries that require challenging manufacturing and implementation processes. We can exemplify the U-shaped waveguide presented by X. Hu in 2014 [93] or the partially tilted waveguide presented by S. Ye et al. in 2017 [94], which are highly sensitive to fabrication errors or do not have current manufacturing methods. Furthermore, the

fabrication processes of structures such as those presented by M. Shah et al. in 2017 [95], X. Zou et al. [88], and Y. Xu et al. in 2019 [96] are complex and have too many steps. Devices such as those of R. Hao et al. 2013 [97] and X. Peng et al. 2015 [98], with multiple layers of graphene, exhibit a high modulation capacity ($1.6\,\mathrm{dB}/\mu\mathrm{m}$), however, issues related to the isolation of layers and the metallization of electrical contacts still exist, hampering their implementation [61, 99]. Since silicon cannot grow directly on graphene [61], graphene-embedded designs, such as those presented by Z. Lu and W. Zhao in 2012 [62], and W. Chen et al. in 2021 [87], have yet to find a simple way to manufacture [91, 97]. Furthermore, most of the devices proposed to date can modulate only in phase or only in amplitude, limiting the applicability.

Therefore, there exists an opportunity for research and development of new designs that are compatible with standard electronics and current manufacturing processes, while simultaneously exhibiting polarization-insensitive optical modulation (in-phase and in amplitude), large operating bandwidth, high speed, low consumption, and a compact structure with low losses.

1.6 Objectives of this work

1.6.1 General Objective

In this work, we are aimed to contribute to the scientific literature with a new design of a polarization-insensitive optical modulator. In particular, we will exploit the unique features of graphene, combined with the optical properties of conventional silicon waveguides, to design a CMOS-compatible optical modulator, insensitive to polarization, with a compact and simple structure that can be easily produced and integrated into photonic circuits, capable of performing amplitude and phase modulation in the same device.

1.6.2 Specific Objectives

- Our main goal is to develop a polarization-insensitive optical modulator.
- Optimize the layout for the highest possible modulation performance.
- Explore amplitude and phase modulation mechanisms.
- Search for the simplest, most compact, and fabrication-friendly structure possible.

1.7 Publications from this work

Below we show the contributions to the literature during the realization of this research work.

❶ **B. N. O. Andrade**, W. O. F. Carvalho, F. Beltrán-Mejia, and J. R. Mejía-Salazar. **Polarization-Insensitive Optical Modulator Based on Single-Layer Graphene Sheets**. *IEEE Transact. Nanotech*, vol. 20, pp. 883-888, 2021.

❷ W. O. F. Carvalho, **B. N. O. Andrade**, J. R. Mejía-Salazar. **Polarization-insensitive optical modulators based on single ENZ-graphene layers**. *Proc. SPIE 11802, Nanoengineering: Fabrication, Properties, Optics, Thin Films, and Devices XVIII* 2021.

1.8 Organization of this dissertation

This dissertation is organized as follows. In Chapter 2, we briefly review the theoretical basis of the main physical effects involved in optical modulation, approach the most common types of modulators, and present some properties of silicon and graphene. In addition, we describe the mathematical model of graphene conductivity used in this work. In Chapter 3, we present the proposed layout and the elements considered in our project. We describe the process of numeric simulation and the definition of the ideal geometric parameters for polarization-insensitive modulation with maximum performance. In addition, we discuss the fabrication methods of the main components of the modulator. In Chapter 4, we analyze the performance of the proposed modulator for modulation in amplitude and phase, determining the modulation depth and the refractive index variation as a function of wavelength and Fermi energy. Also, we calculated the losses, operating frequency, power consumption, and operating bandwidth for both modulation mechanisms (amplitude and phase), considering different modulator lengths. Then we discuss the results, comparing them with other recent projects in the literature. Finally, in Chapter 5, we present the conclusions of this work and the project for future research.

Chapter 2

Review of Theoretical Basis

Modulation consists of the process of altering some physical parameter (amplitude, phase, polarization) of the signal to be transmitted so that it represents a certain logical level (bit) of information [12]. Optical modulating devices can be divided in several ways, such as direct or external modulation, materials, geometries, applications, and/or physical effects involved [36]. This section will review some of these basic concepts.

2.1 Optical Modulation Mecanisms

There are several types of electro-optical effects used for light modulation; the main effects used in optical modulators are:

- **Pockels-effect:** The Pockels-effect occurs when an electric field is applied to a material and causes changes in the index of refraction [12]. It is commonly exploited in Lithium Niobate ($LiNbO_3$) phase modulators, and III-V semiconductors, but is practically negligible in silicon [32]. This effect is sensitive to light polarization and electric field direction [100, 101].
- **Kerr-effect:** The Kerr-effect also results in changes in the material's refractive index, but it depends on the square of the applied electric field [12, 32]. It has a lower intensity than the Pockels-effect and is also used in phase modulators [100, 101].
- **Electro-absorption:** The electro-absorption effect is explored in amplitude modulators [12, 36]. The applied electric field alters the gap between the conduction and valence bands of a semiconductor, modulating the light absorption capacity [102]. There are two physical effects related to electro-absorption: the Franz-Keldysh effect, which occurs in silicon and III-V semiconductors compounds [18, 103]; and the Stark-effect, which occurs in quantum well structures [36, 100–102, 104].

This effect can be wavelength dependent and affected by temperature, depending on the structure and materials involved [12].

- **Carrier density:** Carrier density effects are particularly interesting on silicon, where the electro-optical effects are very weak [18, 32]. By modulating the carrier density it is possible to change the refractive index and the absorption capacity, modulating the optical signal in phase and amplitude [12]. The physical effects involved can be band-filling, band-gap shrinkage, and free-carrier absorption (plasma effect) [100].
- **Interference:** Interference occurs when two or more electromagnetic waves overlap [12]. In an optical communication system, considering monochromatic signals of the same frequency, the interferometric structure can cause constructive or destructive interference, depending on the phase difference between the optical waves [101]. The phase difference can be provoked by the optical path or by a change in the refractive index of the waveguide [32, 105]. Interference is conventionally explored in Mach-Zehnder modulators or structures such as microrings resonators and Fabry-Perot resonant optical cavities [101].

Optical modulators can also use other effects such as magneto-optics, thermo-optics, acousto-optics, etc. [18, 36], but these effects are outside the scope of this dissertation. A more complete description of the presented electro-optical effects and other effects can be found in A.Yariv 2007 [100], S.Chuang 2009 [18], and T.Kawanishi 2022 [103].

2.2 Main Types of Modulators

2.2.1 Direct Laser Modulator

Direct modulation of a laser source is the simplest optical modulation concept [21], combining the functions of the light source and light modulation in a single device [15, 16]. It is based on the direct variation of the laser bias current (electrical input data signal), which interferes with the electrons of the spontaneous/stimulated emission process of the laser, modulating the amplitude of the output signal [12, 17]. This technique produces the simplest and most compact modulating device. The main disadvantage is the inherent and device-specific chirp [18, 21].

The chirp is a variation in the laser's wavelength, leading to distortions and spectral broadening of the signal [15, 36]. This phenomenon occurs due to changes in the refractive index and a series of coupled oscillations (known as relaxation oscillations), caused by variations in the drive current (input signal) of the laser diode [13, 14].

Chirp, along with chromatic dispersion, can cause intersymbolic interference and cross-talk [36, 106, 107], dramatically reducing system performance [108]. It is possible to circumvent these problems through electronic equalization techniques, error correction, and careful engineering of the device, but this increases the complexity, consumption, and costs of the system. Due to the chirp (and limited operating frequency), direct modulation was replaced by external modulation [24], which is done by a device separate from the optical source.

2.2.2 Amplitude modulator

Amplitude modulators use electro-absorption or carrier density effects to modulate optical output signal power [36]. Having a simplified design it can be made from a single waveguide with electrodes that generate the modulating electric field. Amplitude modulators in general have the advantage of being small, highly integrable in optical chips, and can be directly connected to fiber or used in conjunction with Mach-Zehnder interferometers. The main parameters are the modulation depth (or extinction ratio) usually given in dB/μm, insertion losses, operating bandwidth, and 3dB-bandwidth. These values can vary greatly depending on the type of modulator, geometry, and materials used [12].

2.2.3 Phase Modulator

Advanced optical modulation formats often require optical phase modulation [12]. Phase modulation can be performed by manipulating an applied electric field, which modifies the refractive index of the waveguide and changes the propagation velocity of the guided carrier [32]. The effects used can be Pockels-effect, Kerr-effect, carrier density, or even a combination of more than one of these effects. The change in the refractive index depends on the materials, geometry, and direction of the electric field [36]. The most used materials are $LiNbO_3$, gallium arsenide (GaAs), and indium phosphide (InP) [12].

Phase modulators can be used directly, but since common photodetectors are not optical phase-sensitive, demodulation would require coherent optical receivers in conjunction with other expensive and complicated devices and circuits [103]. This is why phase modulators are often used in the arms of the Mach-Zehnder modulator, which converts the phase-modulated signal into an amplitude-modulated signal through an interference structure [36].

2.2.4 Mach-Zehnder Interferometer

The modulation performed through the interferometer Mach-Zehnder deserves a highlight because, in addition to being the first external modulator implemented in long-distance communication systems, it is also the most widespread type of modulator in optical networks [12].

An interferometer Mach-Zehnder modulator (MZM) splits the incoming light into two arms (or branches) in a Y-junction. It then applies electro-optical effects on one or both branches, changing the propagation speed of the guided mode and causing a phase mismatch between the two arms of the modulator. In the third step, both modulator arms are merged, and the recombined signal forms a constructive or destructive interference pattern [101].

MZM can be made from inorganic crystals, polymers, and semiconductors, although the standard material is Lithium Niobate ($LiNbO_3$), with well-developed manufacturing technology [12]. Modern $LiNbO_3$ MZM modulators have a modulation depth superior to 20 dB, with an insertion loss below 5 dB, being able to cover $1525 - 1625$ nm, with a 3dB-bandwidth of 30 GHz, and $10 - 15$ cm long structure [109–111].

This type of modulator is widely used as it offers great modulation depth and is chirp-free [36]. On the other hand, it has a critical intrinsic limitation related to its dimensions [12]. The typical footprint of a Mach-Zehnder modulator varies from millimeters to centimeters, making its use in integrated optical chips impracticable [24, 103]. Therefore, alternatives to MZM are sought for the next generation of optical modulators.

2.2.5 Resonant Modulators

Resonant modulators using Fabry-Perot optical cavities, or ring-shaped resonator structures, are especially attractive for silicon photonics because they have small structures (few millimeters), easy integration, low consumption (< 1 pJ), and good modulation depth (> 1 dB/mm) [37–39]. The structures of this type of modulator are usually very sensitive, small variations in the drive voltage are enough to generate disturbances in the coupling, attenuation, or propagation constant, shifting the resonance and modulating the output signal [18, 32, 40]. Unfortunately, these devices have limited operating bandwidth (few nanometers around the resonance wavelength) and are also highly sensitive to temperature variation [41–43], which hinders their application in many practical scenarios [36, 100].

2.3 Materials Properties

The materials, with which the modulators are made, determine its characteristics, manufacturing processes, and electro-optical effects [18]. It is important to note that not all effects occur on every type of material, although most materials support multiple possibilities [12]. For example, linear and quadratic electro-optic effects occur in dielectrics and semiconductors, on the other hand, electro-absorption and carrier density occur only in semiconductors [32,100]. The ideal material for optical modulators should be transparent at the operating wavelength, have high levels of electro-optical effect, be thermally stable, low loss, low dispersion, and facilitate fabrication methods [12].

As semiconductors accept electro-optical, electro-absorption, and carrier density effects, let's review some properties of this type of material. Semiconductors also facilitate integration with standard electronic components (CMOS), as well as lasers and fiber optics [32]. There are two classes of semiconductors that are relevant for modulators: silicon and III-V semiconductor compounds [12].

2.3.1 III-V Semiconductor Compounds

The III-V semiconductors are composed of elements from group III and group V in the periodic table such as Gallium Arsenide (GaAs) and Indium Phosphide (InP), which are among the most used materials in electro-optic components such as leds, laser diodes, semiconductor optical amplifiers, photodetectors, electro-absorption modulators, and electro-optical switches. These components already have very well-developed optoelectronic manufacturing technology [32].

2.3.2 Silicon

Silicon (Si) is a semiconductor abundant on the planet, it has become the basis of a large microelectronics industry. It is also the most widely used material in optical communications, being the main component of optical fiber. Because it is present in both the electrical and optical domains, silicon is especially attractive for the integration between photonics and electronics. This integration has been the focus of research and development for some time, forming an exclusive area called silicon photonics [32]. Researchers are looking for optical components such as lasers, modulators, and detectors, made from silicon using manufacturing processes that are already used in microelectronics [31]. This would reduce the production cost of electro-optical devices and facilitate integration. Silicon photonics is also expected to advance toward the creation of cost-effective, compact, and efficient Photonic Integrated Circuits (PICs)

capable of outperforming microelectronic circuits [12, 24, 32, 112].

Among the several proposals considered for silicon photonics, the silicon-on-insulator (SOI) made from silicon and silica (SiO_2), is the most used platform for the production of waveguides in optoelectronic components [31]. The high contrast between the refractive indices ($n = 3.5$ for Si and $n = 1.45$ for SiO_2) allows strong confinement of light in waveguides with nanometric dimensions, allowing the creation of dense photonic circuits, reducing costs, and improving device efficiency and performance [32].

However, silicon is limited in terms of electro-optical effects and, except for easy integration with electronics, it would not be a good choice as a modulating material [12]. The linear electro-optic effect (Pockels-effect) is practically null, the Kerr-effect and the Franz-Keldysh effect are also very weak [32]. Low electro-optical effects make it difficult to change the refractive index, and the large band-gap of silicon hinders the absorption, resulting in large and impractical optical modulators for use in PICs [18, 36].

To overcome this problem, current research has shown that a promising path is the hybrid devices of silicon with other materials [46, 47]. This solution combines the advantages of silicon, such as the easy production of waveguides and the high integration with electronics, together with the strong electro-optical effects of different materials [45]. Several materials are easily integrated with silicon waveguides, among the various proposals, two-dimensional materials (2D), such as graphene, have stood out, demonstrating great potential as an active medium for optical modulators [52, 68, 113].

2.3.3 Graphene

Graphene is a two-dimensional (2D) allotrope of carbon, with its atoms arranged in a single plane forming a hexagonal lattice, similar to a honeycomb [114]. With the thickness of a single atom, it is one of the thinnest materials ever synthesized [54, 115]. Due to its exceptional physical properties such as flexibility [116], transparency, chemical stability, and lightness [117], in addition to its high thermal conductivity [118, 119], graphene has been extensively studied since its discovery in 2004 [48, 56]. Moreover, graphene is one of the best electrical conductors that exist [49, 58], making it ideal for applications merging electrical and optical properties in a single device.

In fact, the unique electro-optical properties of graphene, such as strong coupling with light [55, 63], high absorption [58], and tunable optical conductivity [60], have been exploited for emission [120], transmission [121], modulation [38, 70, 71], and detection of optical signals [122, 123]. A single layer of graphene can absorb 2.3% of incident light over a wide spectrum [58, 124] (approximately 50 times the absorption of conventional bulk materials [59, 69]), ranging from far-infrared to ultraviolet, which

covers the bands used in optical communications ($1260 - 1675$ nm) [30, 125]. The electro-optical effect of graphene is some orders of magnitude greater than that of silicon [126, 127], and the thermal conductivity is 100 times greater than Gallium Arsenide (GaAs) [128], widely used in optical components [119]. The high carrier mobility, and the relaxation rate in picoseconds (time taken to the return to natural state after application of an electromagnetic pulse), allow devices to operate at hundreds of GHz without chirp [54, 129]. In addition, its compatibility with conventional electronics makes it a prominent candidate for high-frequency applications [130–132], integrated optical chips [133–135], and the construction of smaller and more efficient devices [76, 136–138].

2.3.3.1 Conductivity Model for Graphene

When integrated with optical waveguides, graphene can strongly interact with the propagation modes [70, 71, 91]. Significantly, this interaction can be modulated by adjusting an externally applied voltage [139]. The principle behind such modulation stems from the electro-optical properties of graphene. Since graphene is a 2D material, i.e., it is an intrinsically anisotropic [140–145], so we have two different models for the permittivity, one for the in-plane and other for the out-of-plane axis. For the in-plane permittivity we use,

$$\varepsilon_{||} = 1 + \frac{i\sigma_{||}}{\omega\varepsilon_0 d_g}, \tag{2.1}$$

in agreement with Refs. [83, 146, 147]. $\sigma_{||}$ indicates the conductivity of graphene, ω the angular frequency, ε_0 the vacuum permittivity, and $d_{\mathrm{g}} = 0.7\,\mathrm{nm}$ corresponds to the thickness of the graphene layer [80, 148]. In contrast to $\varepsilon_{||}$, which takes into account the properties of electrons in the graphene plane, the out-of-plane permittivity $\varepsilon_{\perp} = 2.5$ is considered non-dispersive [94, 142, 149]. These informations can be put together in the permittivity tensor [83, 150, 151],

$$\varepsilon_{x,z} = \begin{bmatrix} \varepsilon_{||} & 0 & 0 \\ 0 & \varepsilon_{\perp} & 0 \\ 0 & 0 & \varepsilon_{||} \end{bmatrix}, \tag{2.2}$$

where the anisotropic feature of graphene is clearly seen.

The graphene's conductivity ($\sigma_{||}$), in the equation (2.1), has a complex value and is formed by the contributions of the intra-band (σ_{intra}) and inter-band (σ_{inter}) conductivities [99, 140, 152], given by:

$$\sigma_{||}(\omega, E_{\mathrm{f}}) = \sigma'_{\mathrm{g}} + i\sigma''_{\mathrm{g}} = \sigma_{\mathrm{intra}} + \sigma_{\mathrm{inter}}, \tag{2.3}$$

which can be modeled with the Kubo formulation [62, 153–155]:

$$\sigma_{||}(\omega, E, \Gamma) = \frac{ie^2(\omega - i2\Gamma)}{\pi\hbar^2}.\left[\frac{1}{(\omega - i2\Gamma)^2}\int_0^\infty E\left(\frac{\partial f(E)}{\partial E} - \frac{\partial f(-E)}{\partial E}\right)dE - \int_0^\infty \frac{f(-E) - f(E)}{(\omega - i2\Gamma)^2 - 4(E/\hbar)^2}dE\right], \tag{2.4}$$

where, ω, Γ, E, and $f(E)$ are the angular frequency, dispersion rate, energy, and the Fermi Dirac distribution function, respectively. The first and second parts of equation (2.4) corresponds, respectively, to the contribution of the intra-band (σ_{intra}) and inter-band (σ_{inter}) conductivities [152].

The dispersion rate (Γ) can be defined by:

$$\Gamma = \frac{1}{2\tau} \tag{2.5}$$

where τ is the electron relaxation time, which dependent on the quality of graphene [78], for a pristine graphene layer can be estimated by [62, 152]:

$$\tau = \mu\frac{E_f}{eV_{\text{f}}^2}, \tag{2.6}$$

being $\mu = 10^4 \text{cm}^2\text{V}^{-1}$ the graphene's carrier mobility, E_f the Fermi's energy, and $V_{\text{f}} = 10^6$ m/s the Fermi's velocity [150, 156].

The Fermi Dirac distribution function is calculated as [112]:

$$f(E) = \left(1 + exp\left[\frac{E - E_f}{k_{\text{B}}T}\right]\right)^{-1}, \tag{2.7}$$

where k_{B}, is the Boltzmann constant and T is the room temperature.

Substituting the equations (2.5) and (2.7) in equation (2.4) and calculating the integrals, σ_{intra} and σ_{inter} can be written as [155]:

$$\sigma_{\text{intra}} = \frac{ie^2k_{\text{B}}T}{\pi\hbar^2(\omega + i\tau^{-1})}\left\{\frac{E_f}{k_{\text{B}}T} + 2\ln\left[\exp\left(\frac{-E_f}{k_{\text{B}}T}\right) + 1\right]\right\}, \tag{2.8}$$

$$\sigma_{\text{inter}} = \frac{ie^2}{4\pi\hbar}\ln\left(\frac{2|E_f| - (\omega + i\tau^{-1})\hbar}{2|E_f| + (\omega + i\tau^{-1})\hbar}\right). \tag{2.9}$$

The optical conductivities of graphene (σ_{intra} and σ_{inter}) can be manipulated by doping with impurities or, more dynamically, by applying an external electrical potential (V) [48, 70]. The electrical voltage modifies the carrier density and changes the Fermi's energy (also called chemical potential), controlling the graphene optical intra/inter-band

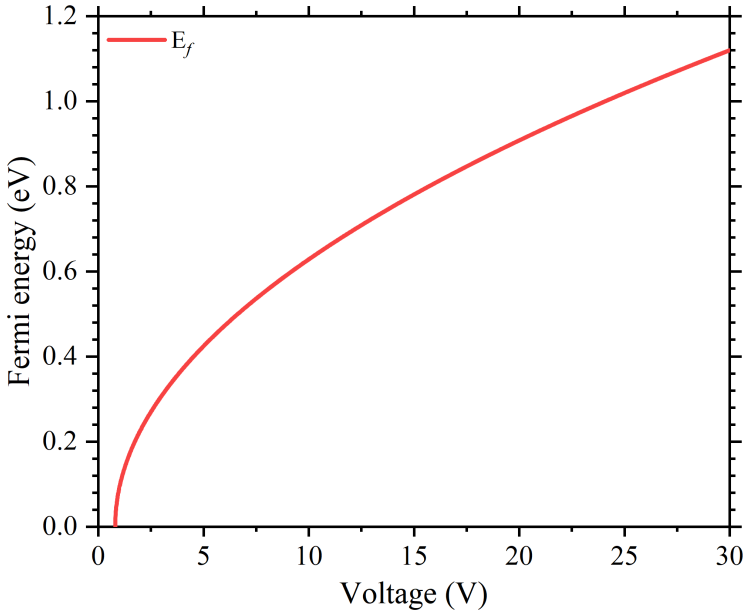

Figure 2.1: *The Fermi's energy as a function of the applied voltage (V), according to the Eq. (2.10)*

transitions [60, 157]. The Fermi's energy (E_f) can be estimated by [70]:

$$E_f = \hbar V_{\mathrm{f}} \sqrt{\pi |\eta|}, \tag{2.10}$$

where, $\hbar$ is the reduced Plank's constant, and η the carrier density (doping level) of graphene is estimated by [155]:

$$\eta = \frac{\varepsilon_0 \varepsilon_{\mathrm{r}} (V_0 - V)}{ed}, \tag{2.11}$$

being, ε_{r} the relative permittivity, V_0 the natural offset voltage of graphene, V the applied voltage, e the charge of electron, and d the thickness of the dielectric layer below the graphene. The relationship between Fermi's energy (Eq. 2.10) and applied voltage V is shown in Figure 2.1.

Figure 2.2 shows the behavior of the real and imaginary parts of $\varepsilon_{||}$ as a function of $\pm E_{\mathrm{f}}$ for the wavelength of $\lambda = 1550\,\mathrm{nm}$. The real part of the permittivity (black line) is related to the change in the effective refractive index and is exploited in electro-refractive modulators (phase modulator), while the imaginary part (red line) is related to the absorption capacity of graphene and is explored in electro-absorption modulators (amplitude modulator) [158].

The energy of Fermi dictates the optical behavior of graphene [159]. For example, for E_f between $\pm\, h\nu/2$, where h is the Planck's constant and ν is the photon's frequency, the electrons in the valence band absorb the photon's energy and are excited to an

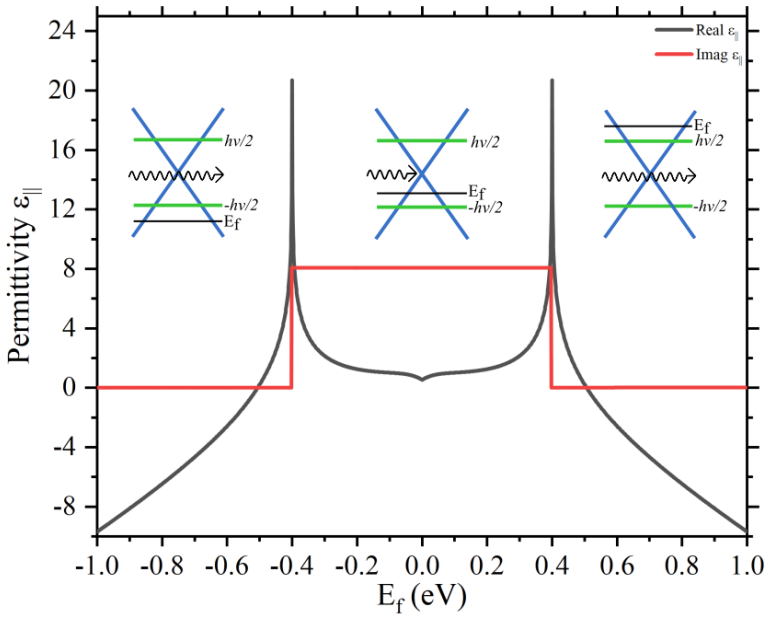

Figure 2.2: *Real and imaginary parts of graphene's in-plane permittivity ($\varepsilon_{||}$) as a function of E_f, according to the Equation (2.1). The inserts show the photon absorption when $-h\nu/2 < E_f < h\nu/2$ and propagation when $-h\nu/2 > E_f > h\nu/2$.*

empty state in the conduction band, this is called inter-band transition [54]. That is, for $\lambda = 1550\,\text{nm}$ and $-0.4 < E_f < 0.4\,\text{eV}$, graphene absorbs the energy of the photons (behaves like an absorber), as shown in the inserts in Fig. 2.2. For $E_f < -0.4\,\text{eV}$ there is an accumulation of positive charges and there are no electrons available for the inter-band transition, so the absorption of the photons no longer occurs. Analogously, for $E_f > 0.4\,\text{eV}$ the accumulation of electrons occupies all states, not allowing inter-band transitions. In both last two situations, the absorption (imaginary part) is practically zero, graphene is then considered transparent to light [54]. This mechanism is called Pauli's blocking, and we exploit this property to switch between ON/OFF states in amplitude modulation.

Chapter 3

Design and Simulations

As we have seen, the feasibility of a graphene-based optical modulator has already been proven [70, 71], and the research on these devices continues to be very active and fruitful [72, 74, 160]. However, most modulators presented in the literature can modulate only one of the fundamental guided modes (TE or TM). In other words, they are devices sensitive to polarization. That is, for their correct functioning, polarization control mechanisms are necessary, which increase the losses, complexity, and cost of the systems [36], in addition to limiting applications and hindering integration with photonic circuits [88, 161]. Modern systems require polarization-insensitive devices. In this sense, new proposals for polarization-insensitive modulators have emerged, such as Refs. [84, 86, 88, 91, 150, 162, 163], demonstrating the feasibility of research and development to expand the applications of this device. The proposals presented have several approaches, however, most have complex designs that require several manufacturing steps and, in addition, can modulate only in amplitude or only in phase. A versatile solution that is capable of doing both types of modulation is very attractive for multiple applications. Thus, we seek to circumvent the limitations of the previous proposals and develop a device insensitive to polarization, with a compact and simple structure, easily manufacturable and integrable with photonic circuits, capable of performing amplitude and phase modulation.

Among the various projects and possibilities analyzed, such as embedded graphene [87], graphene on fiber [81], slot waveguide [86], etc. we chose the silicon-on-insulator (SOI) structure. The SOI structure, based on silicon and silica (SiO_2), is well know and widely used in nanometric components, having a mature manufacturing process, capable of producing waveguides with high precision ($< 10\,\text{nm}$) [15, 31]. For the type of modulator that we are looking for, this is the most suitable platform, due to the simplicity and high confinement capacity of the guided modes [112, 126, 159].

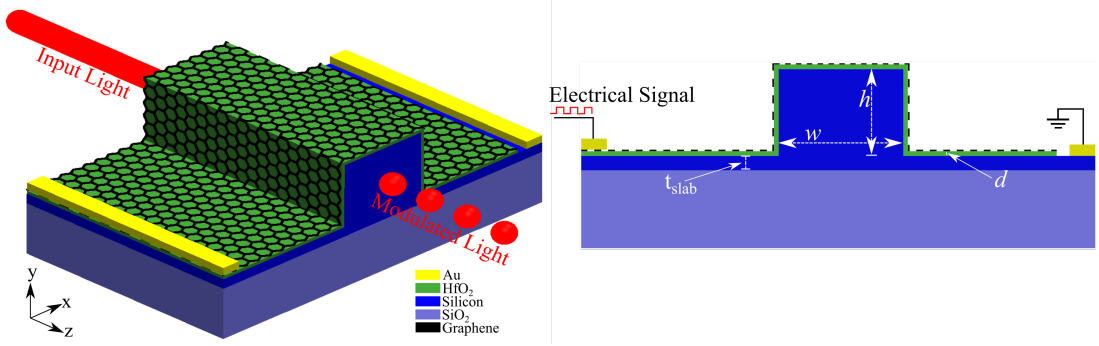

Figure 3.1: *Left figure is a schematic of the graphene-insulator-silicon electro-optical modulator. The right figure shows a cross-section view of the proposed device.*

3.1 Structure

Our design consists of a rectangular Si waveguide in a thin silicon film on a silica (SiO_2) substrate, with a single layer of graphene covering the entire structure, as schematized in Figure 3.1, the left is an isometric view and the right is the cross-section of the proposed modulator. To apply the electrical bias signal, that is, the signal that shifts the Fermi level and dynamically modifies the behavior of graphene, we use two gold (Au) contacts, one being connected to graphene and the other to the silicon film. To avoid unwanted interactions with optical modes, contacts are placed at 600 nm on each side of the waveguide. Between graphene and silicon, we used a thin dielectric spacer made of hafnium dioxide (HfO_2). The HfO_2 is widely used in electro-optical devices as an insulator in capacitive structures due to its high dielectric constant (4-6 times the dielectric constant of silica) [164], and has a practically constant refractive index ($n = 1.87$) throughout the analyzed wavelength range ($1200 - 1700$ nm) [165], which can be implemented with high precision through Chemical Vapor Deposition (CVD) [164]. Notably, this structure does not generate alignment issues, as is often the case with graphene-embedded devices.

3.1.1 Waveguide

Waveguides made of silicon can be easily obtained using standard lithography processes [166–168]. Lithography is a well-known technique, widely used since the 1980s for the large-scale production of integrated circuits and microchips [166]. With well-developed technology, lithography makes it possible to create patterns of sizes ranging from centimeters to a few nanometers (< 10 nm) [167]. The process starts with a mask with the layout of the device to be created, which is deposited on a photoreactive material, after the application of a beam of ultraviolet light (with wavelengths of $13.5 - 436$ nm), the material is dissolved in a developer solvent, leaving the latent

pattern in a type of chemical stencil with the mask image. This stencil then serves as a template for the deposition or engraving processes, which add or remove materials [168]. In industry, the mask covers a large area, allowing the fabrication of a large number of structures simultaneously; a single lithographic machine is capable of producing 100 trillion resources per hour with very high fidelity [24, 168]. The most commonly used techniques are photolithography, soft lithography, and nanoprint lithography [167].

3.1.2 Graphene Layer

As was discussed earlier, graphene is an anisotropic material [140, 141]. That is, the fundamental mode of propagation – TE or TM – which is parallel (in-plane) to the graphene layer is highly influenced by the optical properties of the material, while the mode perpendicular (out-of-plane) to the layers suffers a negligible influence. This induces polarization sensitivity in many devices [142–145]. To consider a device insensitive to polarization, it must be able to cause the same changes in both guided modes [57]. Thus, we need a specially designed structure that compensates for the anisotropic behavior of graphene, or that makes it interact equally with TE and TM [88, 90, 91]. In our design, graphene is deposited on the sides of the waveguide, in parallel and strongly influencing both the TE and TM modes. With ideal proportions, polarization insensitivity can be achieved for amplitude and phase modulations.

Currently, there are several methods to obtain graphene, which can be adopted taking into account costs, complexity, technical resources, production capacity, and sample quality [50, 127, 159]. In general, the most suitable method of obtaining graphene is defined by the application, which also determines the size, quality and purity required [139]. For our case, where pristine monolayer graphene is required, the technique most recommended is the CVD [127], which is commonly used to produce graphene for several other nanodevices [127, 139, 164]. This technique is one of the most promising for the mass production of graphene and can synthesize samples with very high quality over an area of several cm^2 [54]. The method uses a hermetic oven with low pressure at 1000ºC where a gaseous mixture composed mainly of methane (CH_4) is introduced, a reaction with catalysts occurs and the chemical bonds are broken releasing H_2 and depositing the carbon atoms on the metallic plate (made of copper or nickel). When the graphene layer is formed, the film is cooled to room temperature and then transferred to a polyurethane substrate to be deposited at the definitive location, so the substrate is removed by dissolving in acetone [139].

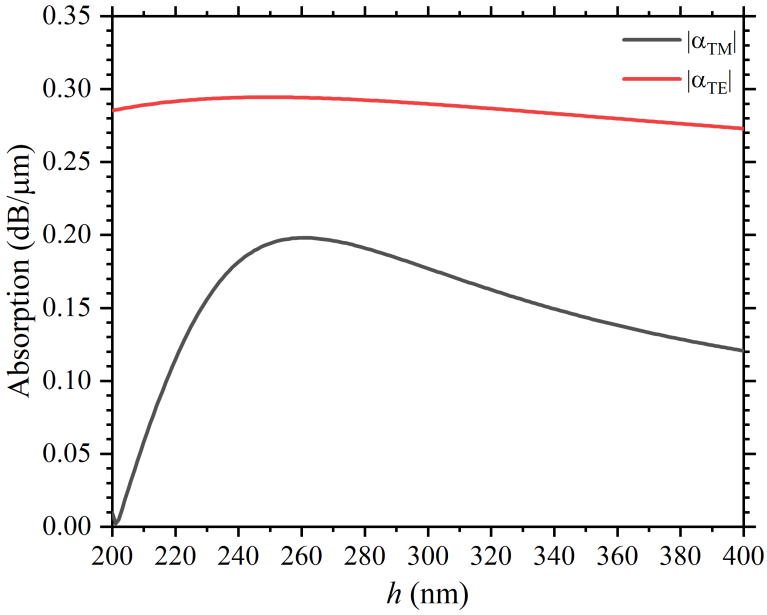

Figure 3.2: *Absorption of TE (α_{TE}) and TM (α_{TM}) modes as function of waveguide's height*

3.2 Study and Optimizations

Several numerical simulations were performed to define the optimal dimensions of the modulator. The studies were done using the Finite Element Method (FEM) through the commercial software COMSOL Multiphysics®. We apply Perfectly Matched Layers (PMLs) at the boundaries of the entire structure to avoid unwanted numerical reflections, customize the mesh to optimize the computational effort, and increase the precision of the studies. Numerical results were processed using MatLab software. The values used for the isotropic refractive indices of the materials were $n_{\mathrm{HfO_2}} = 1.8777$ [165], $n_{\mathrm{Si}} = 3.477$ [98], and $n_{\mathrm{SiO_2}} = 1.444$ [169].

In our modulator, the waveguide directly influences the confinement of the modes and defines the positioning of the graphene layers. With the modulator in the OFF state ($E_f = 0.3\,\mathrm{eV}$) and $\lambda = 1550\,\mathrm{nm}$, we start by analyzing the effects that the waveguide height (h) causes on absorption. To do this, we performed a sweep of h between $200\,\mathrm{nm}$ and $400\,\mathrm{nm}$, as shown in Figure 3.2. We can note that the absorption of the TM mode (α_{TM}) is more sensitive to variations in h than the absorption of the TE mode (α_{TE}). The optimal waveguide height was set at $h = 262\,\mathrm{nm}$, as it has the best approximation of α_{TE} and α_{TM} that helps with polarization insensitivity, as well as results in high absorption for both polarizations, maximizing performance.

Then we study the behavior of the absorption of the modes as a function of the width of the waveguide (w). As shown in Figure 3.3, the absorptions of the modes cross at $w = 245\,\mathrm{nm}$ and $w = 386\,\mathrm{nm}$. That is, at these points, both modes have

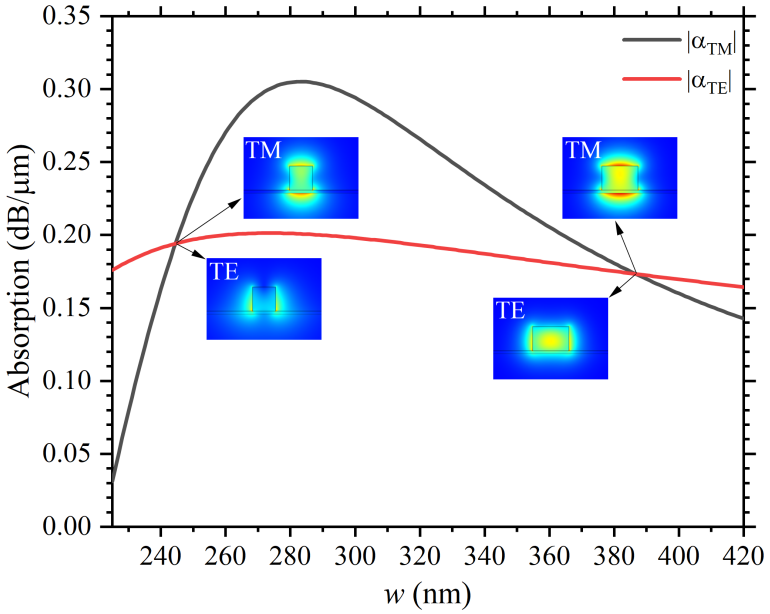

Figure 3.3: *Absorption of TE (α_{TE}) and TM (α_{TM}) modes as function of waveguide's width. The insets show the distribution of the electromagnetic fields of the guided modes.*

the same absorption value, which is essential for polarization-insensitivity. We chose $w = 386\,\text{nm}$ as ideal due to the better confinement of the modes, as demonstrated in the electromagnetic field profiles in the insets of Figure 3.3.

With the waveguide dimensions defined, we started to study the influence of slab thickness (t_{slab}) on the guided modes. As we see in Figure 3.4 the absorption of both modes remains close for $12\,\text{nm} < t_{\text{slab}} < 32\,\text{nm}$. It is also possible to notice an

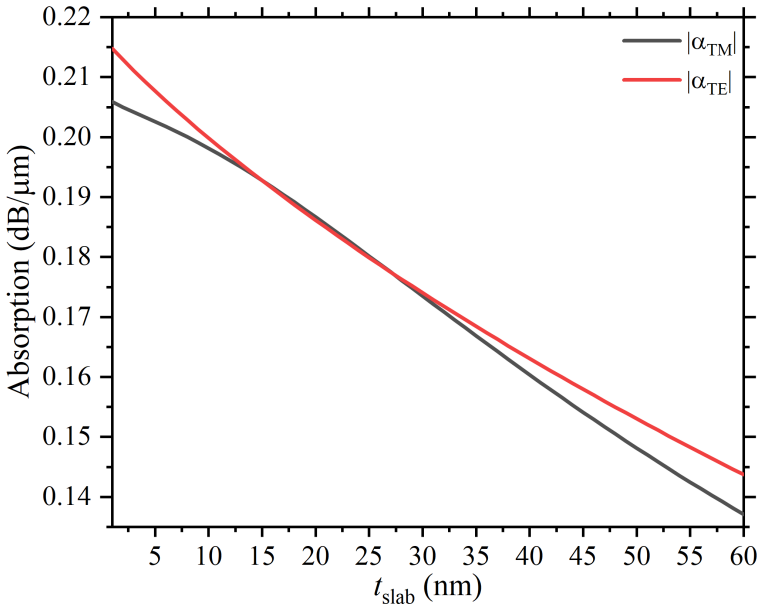

Figure 3.4: *Absorption of TE (α_{TE}) and TM (α_{TM}) modes as function of Slab thickness*

almost linear drop in the attenuations of the modes as the slab thickness increases; this happens because the confined modes begin to move away from the graphene layers, and their energy spreads across the slab. On the other hand, a very thin slab can cause a change in the effective refractive index, generating a divergence of the modes for phase modulation. For this reason, we set $t_{\text{slab}} = 30\,\text{nm}$, keeping the commitment to polarization insensitivity and, at the same time, allowing modulation in amplitude and in phase.

The last parameter to be defined was the thickness of the HfO_2 dielectric spacer. The thickness of the dielectric spacer (d) is an important parameter, as it directly influences the device capacitance and, consequently, other parameters such as energy consumption and 3dB-bandwidth (which will be presented in Chapter 4). Figure 3.5 shows the absorption of guided modes as a function of the thickness of the spacer. We can see that the absorptions of the modes intersect around 7 nm. However, a thinner dielectric spacer would result in lower capacitance and better device performance; on the other hand, it can also compromise the insensibility. Thus, we chose $d = 5\,\text{nm}$ as the ideal thickness, since this value does not compromise polarization insensitivity and, at the same time, optimizes the modulator performance in terms of consumption and bandwidth.

Through Figures 3.3, 3.4, and 3.5, it can be seen that, with other proportions, it is possible to obtain higher levels of absorption, for example $w = 282\,\text{nm}$, $t_{\text{slab}} = 5\,\text{nm}$, or $d = 2\,\text{nm}$. However, the discrepancy between the guided modes rises, increasing the polarization sensitivity. When defining the modulator design, we prioritized polarization insensitivity. In summary, the ideal dimensions for this polarization-insensitive phase

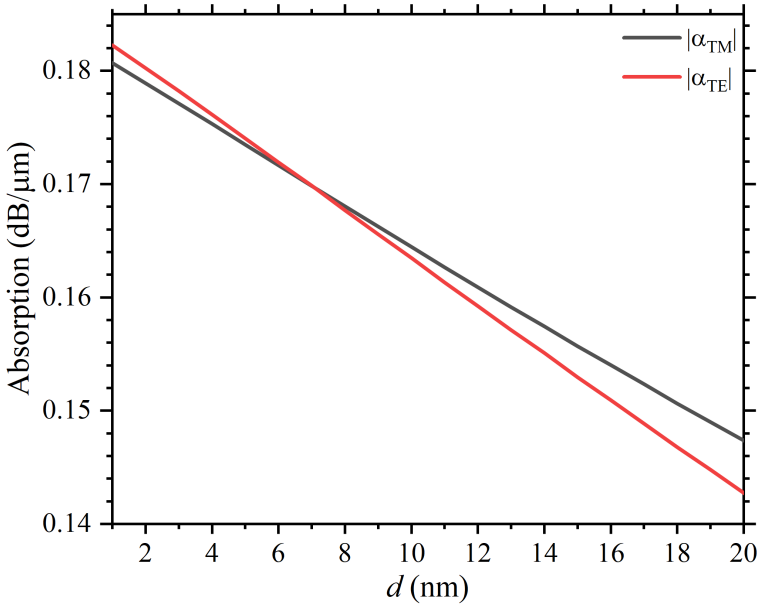

Figure 3.5: *Absorption of TE (α_{TE}) and TM (α_{TM}) modes as function Spacer thickness.*

and amplitude modulator are $h = 262\,\text{nm}$, $w = 386\,\text{nm}$, $t_{\text{slab}} = 30\,\text{nm}$, and $d = 5\,\text{nm}$, as they minimize polarization sensitivity. Other results and analyses of modulator performance are presented in Chapter 4.

Chapter 4

Results and Modulation Performance

In this chapter, we present how changes in graphene properties (adjusted by an externally applied electric field) affect the behavior of guided modes, and we analyze the performance for amplitude and phase modulation.

4.1 Functioning as Amplitude Modulator

Amplitude modulation is one of the most commonly used types of modulation in optical systems [69, 170, 171]. It consists of changing the signal power level, employing electro-absorption or carrier density effects (as previously discussed in Chapter 2) [78,99]. In our device, the amplitude modulation is done by manipulating the absorption capacity of graphene.

Using the optimized geometry, we note that the absorption behavior (as a function of E_f) is almost the same for both guided modes, as shown in Figure 4.1. According to these results, graphene has a high and nearly constant absorption for $E_f < 0.39$ eV, where it drops to close to zero for $E_f \geqslant 0.4$ eV. The difference in absorption for both polarizations ($|\alpha_{\text{TE,TM}}| \approx 1 \times 10^{-3}$ dB/μm) is negligibly small, fulfilling the requirements of a polarization-insensitive amplitude modulator [44, 82].

One of the main parameters for amplitude modulation is the Modulation Depth (MD), defined as the difference between the maximum and minimum absorption of the modes [8, 150]. We define the switching points as 0.3 eV as the state of maximum absorption (OFF state), and 0.5 eV for the state of minimum absorption (ON state), these values were chosen because they are close enough to not compromise energy consumption and, at the same time, can meet all analyzed wavelengths. In the OFF state, the absorptions of TE and TM modes are $|\alpha_{\text{TE}}^{\text{OFF}}| \approx 0.1741$ dB/μm and $|\alpha_{\text{TM}}^{\text{OFF}}| \approx 0.1735$ dB/μm, respectively. In the ON state, the absorptions of the modes are only

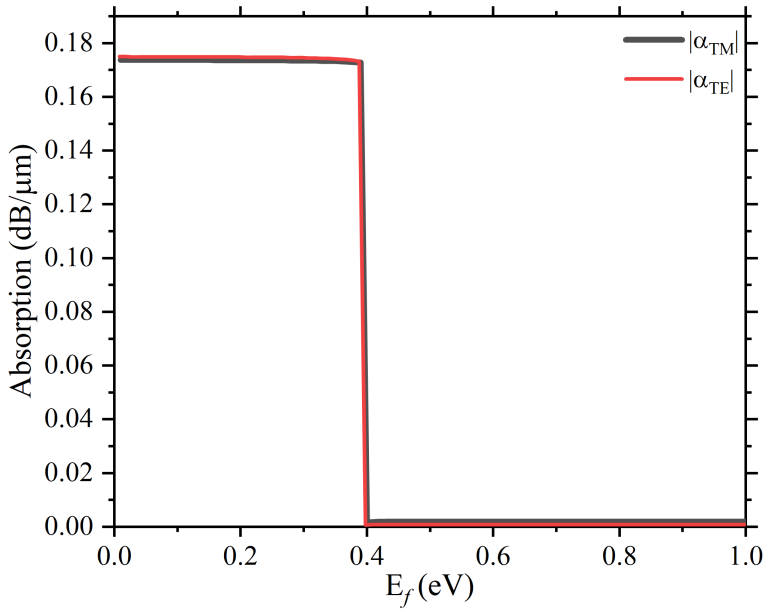

Figure 4.1: *Absorption as a function of E_f for TE (α_{TE}) and TM (α_{TM}) modes for $\lambda = 1550\,nm$.*

$|\alpha_{\text{TE}}^{\text{ON}}| \approx 0.0003$ dB/μm and $|\alpha_{\text{TM}}^{\text{ON}}| \approx 0.002$ dB/μm, as the silicon waveguide has low attenuation, these minimal values were considered as the main loss factor [70]. Therefore, the modulation depth is greater than 0.172 dB/μm for both guided modes. Typically, the 3 dB level is taken as a reference to the minimum acceptable modulation depth [90]. In this way, the minimum length of our design is calculated as $L = \frac{3\text{ dB}}{0.172\text{ dB}.\mu m^{-1}} \approx 17.4\ \mu$m.

4.2 Functioning as Phase Modulator

Phase modulation is performed by the active manipulation of the effective refractive index (n_{eff}) of the guided modes [82, 134, 172, 173]. As shown in Figure 4.2, it is possible to change the n_{eff} by adjusting E_f [41, 97]. We can see that both indexes exhibit almost the same behavior. The largest variation occurs for $0.4 \leqslant E_f \geqslant 1$ eV, being $\Delta n_{\text{eff}}^{TE} = 0.0185$, and $\Delta n_{\text{eff}}^{TM} = 0.0187$, the variations for TE and TM modes, respectively. These values are an order of magnitude higher than the ones for $LiNbO_3$ ($\Delta n_{\text{eff}} = 0.0016$) [174], conventionally used in Mach-Zehnder modulators, which allows us to produce a more compact and energy-efficient device [88, 150]. The difference between the variation of the modes is only 2×10^{-4}, which also fulfills the requirements for polarization-insensitive phase modulation [44, 82].

The phase-change of the modulator is evaluated by [83, 172]:

$$\Delta\phi = \frac{2\pi}{\lambda} L \Delta n_{\text{eff}}. \tag{4.1}$$

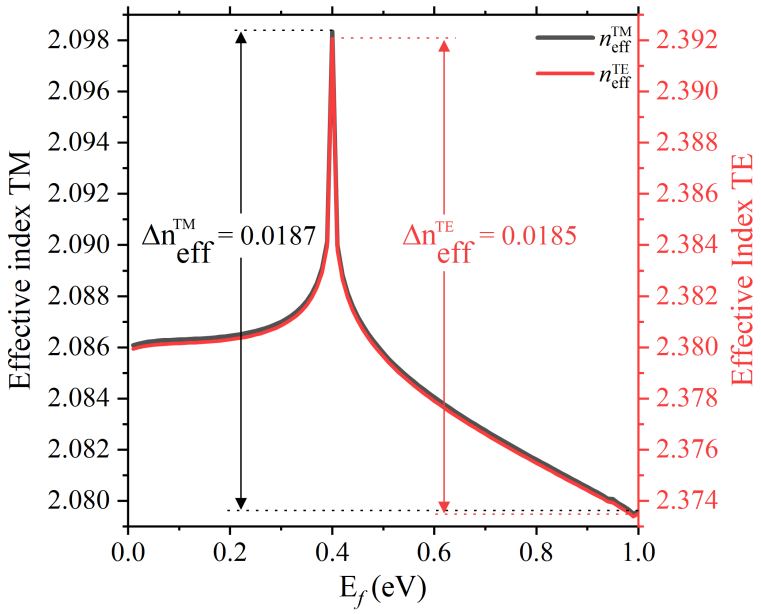

Figure 4.2: *Effective refractive index of TE (n_{eff}^{TE}) and TM (n_{eff}^{TM}) modes as a function of E_f for $\lambda = 1550\,nm$.*

To produce a π-phase change ($\Delta\phi = \pi$), with $\lambda = 1550$ nm, this modulator must be at least $L = 41.7$ μm long, as shown in Figure 4.3 (red lines). For longer modulators, the Δn_{eff} needed for a π-phase shift is smaller, and consequently, the required Fermi energies are also smaller. This last result can be seen from Figure 4.3, where the phase change is shown as a function of E_f for different modulator lengths (considering that the

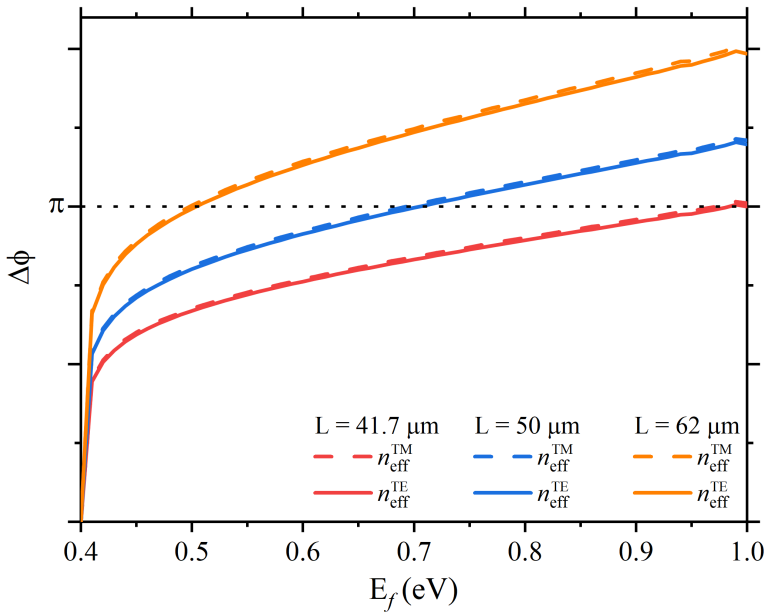

Figure 4.3: *Phase-shift ($\Delta\phi = \pi$) as a function of E_f for different modulator's lengths. $L = 41.7$ μm (red lines), $L = 50$ μm (blue lines) and $L = 62$ μm (orange lines). $E_f = 0.4\,eV$ corresponds to the zero-phase change value.*

phase change at $E_f = 0.4$ eV is zero). As can be seen, a 50 μm (blue lines) modulator can make a π-phase shift with $E_f < 0.7$ eV, while a 62 μm (orange lines) needs E_f only up to 0.5 eV.

An important parameter in optical modulators is the signal loss, which in the proposed design is mainly due to the losses caused by the graphene layer [70, 91]. As observed from results in Figures 4.1 and 4.2, our concept can be used to achieve maximum changes in the effective refractive index with minimum signal losses. In fact, for the region of maximum variation of the effective index ($0.4 < E_f < 1$ eV), the attenuation caused by graphene is quite low and practically constant. In particular, the signal loss for this phase modulator is considered the same as for the amplitude modulator in the ON state, which remains below 2×10^{-3} dB/μm [70]. Since the operating voltages are different, it is possible to perform amplitude/phase modulations on the same device and can be easily implementable through standard CMOS technology.

When operating as an amplitude modulator, the electrical voltage applied to the modulator also changes (in a lesser extent) the effective refractive index, causing an unwanted delay in light propagation. This delay is interpreted as a change in the signal phase. In practical terms, this phase shift can often be negligible, since it is quite low ($\Delta\phi \leq 0.03\pi$) and photodetectors only detect the amplitude of the signal. In case of very sensitive applications involving MZM, it can be easily compensated by designing the optical path, but if the device is applied in cascaded with other modulators in large photonic circuits with higher levels of modulation, may be needed to take into account this effect [103].

4.3 Operating Bandwidth Range

The operating bandwidth refers to the range of wavelengths over which a modulator can maintain its performance. The modern optical communication systems, based on Wavelength Division Multiplexing (WDM), require versatile optical modulations for multiple wavelengths [107, 136, 175], which remarks the importance to analyze the range of operating bandwidth of our device.

For the modulator in the OFF state, we studied the behavior of MD as a function of λ for different modulator lengths, as shown in Figure 4.4. In order to preserve the polarization-insensitive characteristic, the discrepancy between the TE and TM modes must be less than 1 dB (colored dotted lines) [150]. As we can see, for a minimum length of 17.4 μm (red lines), the device is capable of operating above 3 dB of modulation for a wavelength from 1540 to 1670 nm. In the case of longer structures, the operating

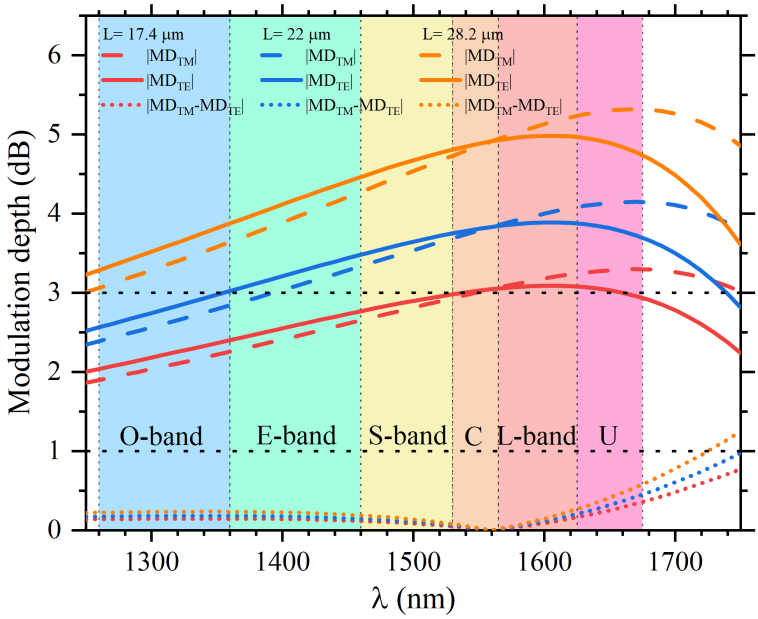

Figure 4.4: *Modulation depth (MD) for TE and TM modes as a function of wavelength for different modulator's lengths:* $L = 17.4\,\mu m$ *(red lines)* , $L = 22\,\mu m$ *(blue lines) and* $L = 28.2\,\mu m$ *(orange lines). The* $|MD_{TE,\,TM}|$ *must be above* 3 *dB, and* $|MD_{TE} - MD_{TM}| < 1$ *dB.*

range is wider, that is, with a length of 22 μm (blue lines) the device works from 1390 to 1740 nm, and with a length of 28.2 μm (orange lines) works from 1240 to 1730 nm. Therefore, with a few micrometers, our device, acting as a polarization-insensitive amplitude modulator, can cover the entire optical communications window [108, 176], beyond the O and U-bands, with the potential to meet upcoming technologies [57, 177].

For phase modulation, the Δn_{eff} changes depend on the wavelength [74, 178, 179]. According to Figure 4.5a, the value of Δn_{eff} decreases for smaller λ, requiring compensation in the modulator length, according to Eq. (4.1). The variations for both modes remain close until $\lambda = 1650$ nm when the discrepancy exceeds 1×10^{-3} and the device becomes polarization sensitive [88]. So, this device can modulate in phase with polarization-insensitivity for $1200 < \lambda < 1650$ nm. Figure 4.5b shows the behavior of n_{eff} for $\lambda = 1250, 1550$, and 1650 nm.

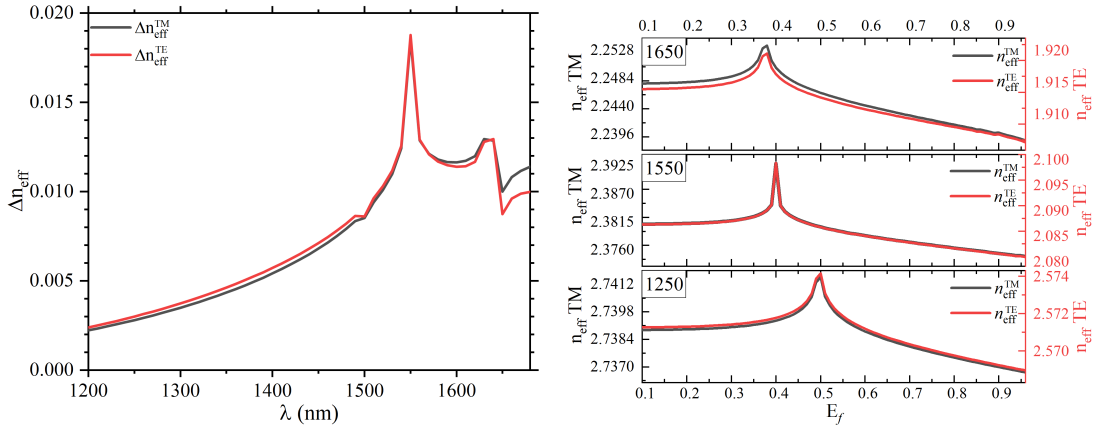

(a) Δn_{eff} *as a function of* λ (b) n_{eff} *as a function of* E_f *for different* λ

Figure 4.5: *(a) Variation of effective refractive index* (Δn_{eff}) *for TE and TM modes as a function of* λ *(nm). (b) Effective refractive index* (n_{eff}) *of both modes as a function of* E_f *for* $\lambda = 1250, 1550,$ *and* 1650 *nm*

4.4 Energy Consumption

Another important parameter to consider is the energy consumption, which is relevant not only for on-chip hardware [135, 180] but also for more energy-efficient and more environmentally friendly systems [181]. To estimate the consumption of the modulator, we use the energy per bit (E_{bit}) parameter [67, 90], calculated as:

$$E_{\text{bit}} = \frac{1}{4} C(\Delta V)^2, \tag{4.2}$$

where ΔV is the voltage required by the modulator (according to Eq. 2.10), $C = \varepsilon_0 \varepsilon_r A_{\text{gra}}/d$ is the total capacitance of the device, obtained by a simple model of a parallel plate capacitor [83, 90, 178], being d the thickness of the dielectric layer below the graphene, and $A_{\text{gra}} = w_g \times L$ the total area of graphene, where $w_g = 2.11\ \mu$m is the effective width and L the length of modulator. The 1/4 factor comes from the Non-Return-to-Zero (NRZ) signaling scheme where, for a random bit sequence, the occurrence of ON/OFF states has the same possibility, and a complete cycle occurs on average once every four bits [182].

In amplitude modulation, the voltage required to switch between ON/OFF states is constant ($\Delta V = 3.72$ V), but the capacitance C increases with the length of the modulator. For a device's length of $L = 17.4\ \mu$m, $L = 22\ \mu$m, and $L = 28.2\ \mu$m, the energy per bit is $E_{\text{bit}} = 0.79$ pJ/bit, $E_{\text{bit}} = 1$ pJ/bit and $E_{\text{bit}} = 1.28$ pJ/bit, respectively. Therefore, there is a trade-off between the wavelength operating range, which is greater for longer modulators (Figure 4.4), and the device's energy consumption.

On the other hand, for phase modulation, the energy expended for a π-phase shift

varies according to the length of the modulator. As shown in Figure 4.3, the energy required for the phase change is lower for longer modulators, resulting in reduced energy consumption. For a modulator with a length of $L = 41.7$ μm, the consumption of energy per bit is $E_{\text{bit}} = 51.88$ pJ/bit. For $L = 50$ μm, and $L = 62$ μm, the energy per bit drops to $E_{\text{bit}} = 9.71$ pJ/bit and $E_{\text{bit}} = 0.9$ pJ/bit, respectively. Although the increase in the area of the device also increases C, the reduction in E_f is much faster, thus allowing us to decrease the energy consumption of the phase modulator at the cost of increasing its footprint.

Table 4.1: *Comparison of the device working as an amplitude and phase modulator with different lengths.*

Modulation	L (μm)	Capacitance (pF)	ΔV (V)	E_{bit} (pJ/bit)	Loss (dB)
Amplitude	17.48	0.23	3.72	0.79	35×10^{-3}
	22	0.29		1	44×10^{-3}
	28.2	0.37		1.28	56.4×10^{-3}
Phase	41.7	0.54	19.56	51.88	83.4×10^{-3}
	50	0.65	7.68	9.71	100×10^{-3}
	62	0.81	2.1	0.9	124×10^{-3}

Therefore, in addition to being able to optimize the modulator's cross-section, we can also optimize the energy consumption by tuning the length of the modulator. In Table 4.1, we summarize the results for the device working as an amplitude and phase modulator with different lengths.

4.5 3dB-Bandwidth

Due to the ultrahigh carrier mobility of graphene, the modulation bandwidth is mainly limited by the parasitic effects of the device (RC delay) [60, 61, 70]. To estimate the 3 dB-bandwidth, it is considered the drop in the modulator response of 3-dB in relation to the peak value, typically uses the $f_{3\,\text{dB}}$, the same parameter used to determine the cutoff frequency of a low pass filter, calculated as [67]

$$f_{3\,\text{dB}} = \frac{1}{2\pi RC}, \tag{4.3}$$

where R represents the total resistance of the device, obtained by [63, 172, 183]

$$R = \frac{2}{L}(R_{\text{s}} w_{\text{g}} + R_{\text{c}}), \tag{4.4}$$

with $R_{\text{s}} = 200\ \Omega$ for the graphene sheet resistance [183], $w_{\text{g}} = 2.110$ μm the effective width of graphene, and $R_{\text{c}} = 100\ \Omega \cdot \mu$m the electrode contact resistance [172, 183].

We reach $f_{3\,\mathrm{dB}} = 11.57$ GHz for both types of modulation. Future developments in graphene deposition and the electrical contacts can improve $f_{3\mathrm{dB}}$ through reduction of R_s and R_c [184, 185].

4.6 Discussion of Results

From the results, we can compare the performance of our device with other modulators presented in the literature. In Table 4.2 we show the results of some polarization-insensitive modulators. Our structure is the unique that uses only a single layer of graphene and is one of the few capable of modulating the amplitude and phase. We can see that our proposal is among the smallest, due to the good modulation depth and the high Δn_eff achieved. The operating bandwidth of 130 nm for amplitude modulation and 450 nm for phase modulation is a notable result, even more considering that we are committed to a more compact structure, these results can be even better for longer structures, as commented on in Section 4.3. The consumption per bit for the amplitude modulation is remarkably low, although the consumption for the phase modulation is a little higher, it is possible to reduce the Ebit by adjusting the modulator length, being able to get below 1 pJ/bit, as commented in Section 4.4. The $f_{3\mathrm{dB}}$ (or 3dB-bandwidth) achieved is reasonable, considering that we used strict parameters for the calculation and, according to V. Sorianello et al. [74], the technological development of graphene contacts and deposition methods can improve this value, making it possible for devices like this to operate above 100 GHz.

Table 4.2: *Comparison of results with the literature.*

	Year	Scheme	L (μm)	MD (dB/μm)	$\Delta Neff$	Bandwidth (nm)	Ebit (pJ/bit)	$f_{3\,\mathrm{dB}}$(GHz)
This Work	2021	Amplitude and phase modulator with a single graphene layer covering a Si rib waveguide	17.48 41.7	0.172	0.0185	1540-1670 1200-1650	0.79 19.56	11.57
[87]	2021	Amplitude and phase modulator with two graphene's layers embedded in SiN waveguide	200	0.1	0.0233	1100-1645	0.687	53
[86]	2021	Amplitude modulator with two graphene's layers in a T-slot waveguide	10	0.371		1460-1620	2.07	50.7
[88]	2019	Phase modulator with two graphene's layers embedded in a Si waveguide	60		0.013	1300-1800		135.6
[96]	2019	Amplitude modulator with multi-layers of graphene embedded in a Si waveguide	20	1.11		1367-1668	7.8	6.1
[84]	2019	Coupling structure and guided mode conversion for amplitude modulation	270	0.063		1500-1600		14.3
[90]	2018	Amplitude and phase modulator with two graphene's layers covering a Si rib waveguide	10.35 164.9	0.29	0.0047	1530-1565	2.98 4.6	30.2
[163]	2017	Amplitude modulator with two graphene's layers embedded in a Si waveguide	12	1.57		1500-1590	0.001	62.74

Chapter 5

Conclusions and Future Research

Summarizing, we propose a polarization-insensitive graphene-based optical modulator, capable of modulating in amplitude or in phase using the same nanostructure. Our device is composed of a single graphene layer over a SOI structure, with a rib-type silicon waveguide upon a silicon slab and a silica substrate. We used a dielectric spacer made of HfO_2 between the graphene and silicon, and two gold contacts spaced from the waveguide, as schematized in Fig. 5.1.

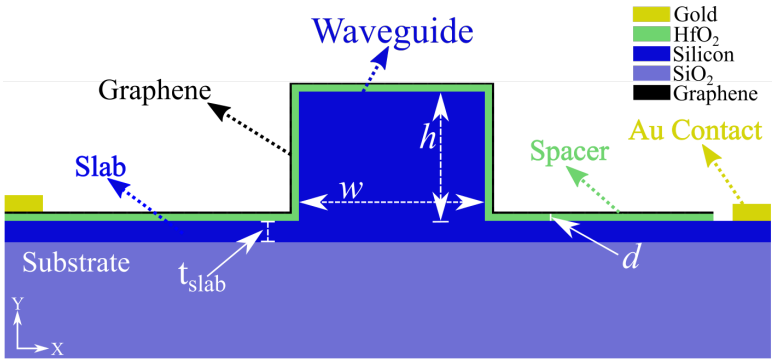

Figure 5.1: *Modulator cross-section schematic*

Our design was optimized for polarization insensitivity and performance. The dimensions are summarized in Table 5.1, which also presents the refractive index of the materials and some graphene parameters that were used for the studies. More information can be found in Chapters 2 and 3.

Table 5.1: *Summary of Modulator Design Parameters*

Structure		Refractive index		Graphene	
Waveguide	h = 262 nm w = 386 nm	HfO_2	n_{eff} = 1.877	Thickness	$d_g = 0.7$ nm
Slab	t_{slab} = 30 nm	Silicon	n_{eff} = 3.477	Carrier mobility	$\mu = 10^4 \text{cm}^2\text{V}^{-1}$
Spacer	d = 5 nm	Silica	n_{eff} = 1.444	Fermi Velocity	$V_f = 10^6$ m/s

The Table 5.2 summarizes some results found in Chapter 4 for amplitude and phase modulation with different modulator lengths operating with $\lambda = 1550$ nm.

Table 5.2: *Summary of Results*

Modulation	Length (μm)	Absorption (dB)	Phase $\phi(\pi)$	Operating Band	E_{bit}(pJ/bit)
Amplitude	17.48	3	0.03π	1540-1670	0.79
	22	3.8	0.03π	1390-1740	1
	28.2	4.88	0.04π	1240-1730	1.28
Phase	41.7	0.083	π	1200-1650	51.88
	50	0.1			9.71
	62	0.124			0.9

Other results include:

- Modulation depth of 0.172 dB/μm.
- Change of refractive index of $\Delta n_{\text{eff}} = 0.0185$.
- 3dB-Bandwidth = 11.57 GHz.
- Difference between the TE and TM modes of 1×10^{-3} dB/μm for amplitude modulation and 2×10^{-4} for phase modulation.

From these results, we conclude that (through a very simple geometrical design) we show a new concept for electro-optical polarization-insensitive modulator using a single graphene layer, capable of modulating in amplitude and in phase. Our proposal is compact, simple to manufacture, compatible with standard electronics, and with no alignment issues. The nanostructure was optimized using numerical simulations prioritizing the polarization insensitivity for both types of modulation (amplitude and phase). In particular, we studied the attenuation and the effective refractive index as a function of E_f, λ, and different modulator lengths. For amplitude modulation, we achieve a modulation depth greater than 0.17 dBμm, with energy consumption below 0.79 pJ/bit and operating bandwidth from 1200 to 1730 nm, capable of covering the entire optical communication window (while maintaining polarization insensitivity) beyond the O and U-bands ($1260 - 1675$ nm), with the potential to meet future technologies. For the phase modulation, we achieved a high change in the effective refractive index ($\Delta n_{\text{eff}} > 0.0185$), allowing a more compact and energy-efficient device. With a

length of a few micrometers, the energy consumption of the fase modulator is below 0.9 pJ/bit, being able to cover from $1200 - 1650$ nm. The calculated insertion loss is just 2×10^{-3},dBμm. The 3dB-bandwidth is 11.57 GHz, for both types of modulation. Notably, the operating voltages for both modulation mechanisms are different, so it is possible to perform amplitude/phase modulations on the same device through adjustments in the power supply drive. In addition, we numerically demonstrate that performance and power consumption can be optimized depending on the application. Since the simulations were performed with experimentally implementable geometries and materials, we expect that the proposed project will arouse significant interest for future applications of optical and photonic circuits.

5.1 Future Research

The electro-optical modulator presented in this work is committed to polarization insensitivity, miniaturization, and the facility of fabrication for integration into photonic circuits. Few proposals in the literature address polarization insensitivity, which leads to the necessity for polarization controller devices, increasing insertion and coupling losses, in addition to complexity and costs. The most current proposals have taken this into account, proving the feasibility of solving this problem. In addition, we were able to address another point that still needs further development, the ability to modulate amplitude and phase in the same structure. This feature gives our device versatility and the ability to meet different applications.

From the studies of the electro-optical modulator presented in this work, it was possible to see more clearly other needs and technological trends. Most of the optical modulators based on two-dimensional materials presented, in addition to the limitations already mentioned, also cling to simple binary modulation schemes, and few explore the possibility of more complex modulations. To meet the growing data traffic demand and future technologies, it is interesting to be able to execute higher-order modulation schemes, as is already explored in conventional semiconductor-based modulators [186–190]. Modulation schemes such as M-PSK (Multilevel Phase Shift Keying), M-PAM (Multilevel Pulse Amplitude Modulation), and M-QAM (Multilevel Quadrature Amplitude Modulation), are currently obtained through cascaded Mach-Zehnder modulators [12, 191–195]. The higher the modulation order, the more intricate and complex the photonic circuits and drive circuits are, which leads to problems of signal loss, coupling losses, chirp, dispersion, in addition to the limitations of electronic circuits.

As the graphene-based modulator has already proven itself to be a worthy substitute

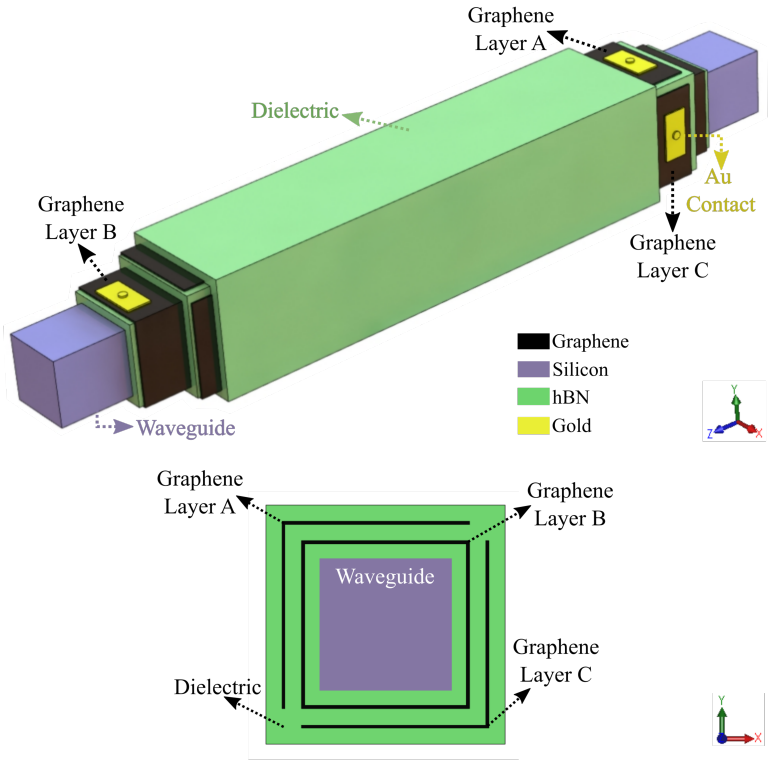

Figure 5.2: *Schematic of a multilevel optical modulator based on graphene. Above the isometric view, below the cross-section of the device.*

for MZM, graphene-based devices for higher modulation levels seem attractive and are beginning to appear in the literature as Ref. [188, 189]. In this sense, we are developing a new graphene-based modulator, capable of performing more complex modulations schemes such as M-PAM, M-PSK, M-QAM, in a single polarization-insensitive structure. Figure 5.2, shows the schematic of the modulator under development, above an isometric view, and below the cross-section of the device. The modulator is composed of an undoped Si waveguide in a rectangular shape, three layers of graphene, and a dielectric spacer. The three layers of graphene are placed around the waveguide, the inner layer surrounds the entire guide, and two other layers cover two sides of the guide each, they are separated to form two capacitive structures. The modulator works by combining the ON/OFF states of the graphene layers, achieving different levels of modulation.

The results obtained so far are very promising. Figure 5.3 shows the different amplitude levels of TE and TM modes achieved through different combinations of graphene layers. A similar effect occurs for phase modulation. Figure 5.4 shows different levels of change in the effective refractive index for different combinations of graphene layers. Figure 5.5 shows the absorption behavior of guided modes along the waveguide for some layer combinations. Notably, our device can operate between

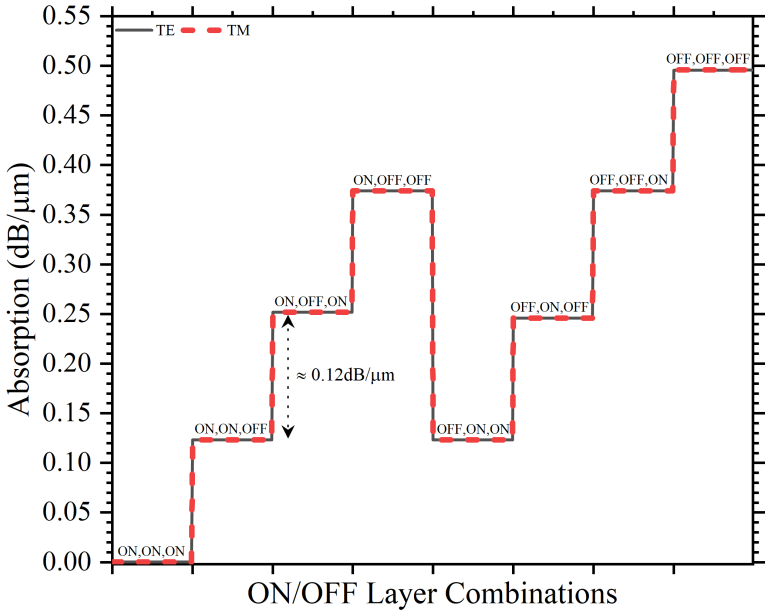

Figure 5.3: *Absorption levels as a function of the ON/OFF combination of layers.*

$1200 - 1750$ nm, with losses below 2×10^{-4} dB/μm, and length of only 16.7 μm. Other points are still under development, including what the fabrication process of such a structure would look like.

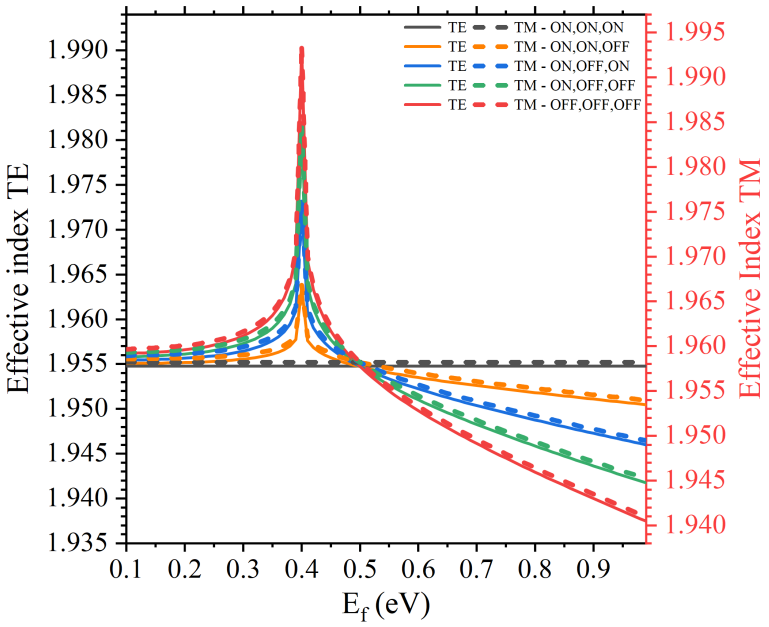

Figure 5.4: *Effective refractive index as a function of the ON/OFF combination of layers.*

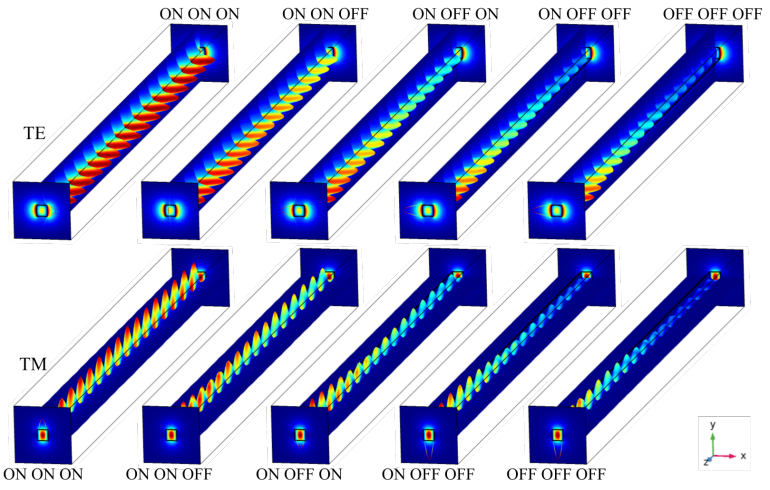

Figure 5.5: *Behavior of propagation of TE and TM modes along the modulator as a function of the ON/OFF combination of layers.*

Bibliography

[1] Cisco, "Cisco Annual Internet Report (2018-2023) white paper," 2020.

[2] Ericsson, "Ericsson Mobility Report white paper," 2020.

[3] T. Nagatsuma, G. Ducournau, and C. C. Renaud, "Advances in terahertz communications accelerated by photonics," *Nature Photonics*, vol. 10, no. 6, pp. 371–379, 2016.

[4] Y. Salamin, B. Baeuerle, W. Heni, F. C. Abrecht, A. Josten, Y. Fedoryshyn, C. Haffner, R. Bonjour, T. Watanabe, M. Burla, D. L. Elder, L. R. Dalton, and J. Leuthold, "Microwave plasmonic mixer in a transparent fibre-wireless link," *Nature Photonics*, vol. 12, no. 12, pp. 749–753, 2018.

[5] S. Ummethala, T. Harter, K. Koehnle, Z. Li, S. Muehlbrandt, Y. Kutuvantavida, J. Kemal, P. Marin-Palomo, J. Schaefer, A. Tessmann, S. K. Garlapati, A. Bacher, L. Hahn, M. Walther, T. Zwick, S. Randel, W. Freude, and C. Koos, "THz-to-optical Conversion in Wireless Communications Using an Ultra-broadband Plasmonic Modulator," *Nature Photonics*, vol. 13, no. 8, pp. 519–524, 2019.

[6] M. Burla, C. Hoessbacher, W. Heni, C. Haffner, Y. Fedoryshyn, D. Werner, T. Watanabe, H. Massler, D. L. Elder, L. R. Dalton, and J. Leuthold, "500-ghz plasmonic mach-zehnder modulator enabling sub-thz microwave photonics," *APL Photonics*, vol. 4, no. 5, 2019.

[7] T. Nagatsuma, S. Horiguchi, Y. Minamikata, Y. Yoshimizu, S. Hisatake, S. Kuwano, N. Yoshimoto, J. Terada, and H. Takahashi, "Terahertz wireless communications based on photonics technologies," *Optics Express*, vol. 21, no. 20, pp. 23 736–23 747, 2013.

[8] G. T. Reed, G. Mashanovich, F. Y. Gardes, and D. J. Thomson, "Silicon Optical Modulators," *Nature Photonics*, vol. 4, no. 8, pp. 518–526, 2010.

[9] Z. Sun, A. Martinez, and F. Wang, "Optical Modulators With 2D Layered Materials," *Nature Photonics*, vol. 10, no. 4, pp. 227–238, 2016.

[10] A. H. Atabaki, S. Moazeni, F. Pavanello, H. Gevorgyan, J. Notaros, L. Alloatti,

M. T. Wade, C. Sun, S. A. Kruger, H. Meng, K. Al Qubaisi, I. Wang, B. Zhang, A. Khilo, C. V. Baiocco, M. A. Popović, V. M. Stojanović, and R. J. Ram, "Integrating Photonics With Silicon Nanoelectronics for the Next Generation of Systems on a Chip," *Nature*, vol. 556, no. 7701, pp. 349–354, 2018.

[11] M. Rahm, J.-S. Li, and W. J. Padilla, "THz Wave Modulators: A Brief Review on Different Modulation Techniques," *Journal of Infrared, Millimeter, and Terahertz Waves*, vol. 34, no. 1, pp. 1–27, 2013.

[12] A. Chen and E. E. Murphy, *Broadband Optical Modulators: Science, Technology, and Applications*, 1st ed. CRC Press, 2012.

[13] I. P. Kaminow and E. H. Turner, "Electrooptic Light Modulators," *Applied Optics*, vol. 5, no. 10, p. 1612, 1966.

[14] L. Allen and A. Muriel, *Essentials of Lasers*, 1st ed. Pergamon Press, 1969.

[15] J. Piprek, *Semiconductor Optoelectronic Devices: Introduction to Physics and Simulation.*, 1st ed. Academic Press, 2003.

[16] T. Paoli and J. Ripper, "Direct modulation of semiconductor lasers," *Proceedings of the IEEE*, vol. 58, no. 10, pp. 1457–1465, 1970.

[17] J. Hecht, *City of Light: The Story of Fiber Optics*, 1st ed. Oxford University Press, 2004.

[18] S. L. Chuang, *Physics of Photonic Devices*, 2nd ed. John Wiley Sons, 2009.

[19] R. W. Burns, *Communications: an International History of the Formative Years*. London Institution of Engineering and Technology, 2004, vol. 2.

[20] R. C. Alferness, H. Kogelnik, and T. H. Wood, "The evolution of optical systems: optics everywhere," *Bell Labs Technical Journal*, vol. 5, no. 1, pp. 188–202, 2000.

[21] M. Csele, *Fundamentals of light sources and lasers*, 1st ed. John Wiley Sons, 2005.

[22] B. A. Horwitz and F. J. Corbett, "The PROM - Theory and Applications for the Pockels Readout Optical Modulators," *Optical Engineering*, vol. 17, no. 4, pp. 353–364, 1978.

[23] H. Bassen and G. Smith, "Electric Field Probes–A Review," *IEEE Transactions on Antennas and Propagation*, vol. 31, no. 5, pp. 710–718, 1983.

[24] M. D. Al-Amri, M. M. El-Gomati, and M. S. Zubairy, *Optics in Our Time*, 1st ed. Springer International Publishing, 2016.

[25] N. Margalit, C. Xiang, S. M. Bowers, A. Bjorlin, R. Blum, and J. E. Bowers,

"Perspective on the future of silicon photonics and electronics," *Applied Physics Letters*, vol. 118, no. 220501, pp. 1–10, 2021.

[26] G. T. Reed and C. Jason Png, "Silicon optical modulators," *Materials Today*, pp. 40–50, 2005.

[27] M. Koziol, "How the Internet Can Cope With the Explosion of Demand for 'Right Now' Data During the Coronavirus Outbreak - IEEE Spectrum," 2020, Accessed in 2022-03-16. [Online]. Available: https://spectrum.ieee.org/everyone-staying-home-because-of-covid19-is-targeting-the-internets-biggest

[28] D. K. Gramotnev and S. I. Bozhevolnyi, "Plasmonics beyond the diffraction limit," *Nature Photonics*, vol. 4, no. 2, pp. 83–91, 2010.

[29] ITRS, "International Technology Roadmap for Semiconductors," Tech. Rep., 2015.

[30] X. Wang and B. Sensale-Rodriguez, "Graphene Based Optical Interconnects," in *Nanoelectronics*. Elsevier, 2019, pp. 271–285.

[31] M. A. Giambra, V. Mišeikis, S. Pezzini, S. Marconi, A. Montanaro, F. Fabbri, V. Sorianello, A. C. Ferrari, C. Coletti, and M. Romagnoli, "Wafer-Scale Integration of Graphene-Based Photonic Devices," *ACS Nano*, vol. 15, no. 2, pp. 3171–3187, 2021.

[32] G. T. Reed, *Silicon Photonics*, 1st ed. John Wiley and Sons, 2008.

[33] D. Miller, "Optical interconnects to silicon," *IEEE Journal of Selected Topics in Quantum Electronics*, vol. 6, no. 6, pp. 1312–1317, 2000.

[34] R. Soref, "The Past, Present, and Future of Silicon Photonics," *IEEE Journal of Selected Topics in Quantum Electronics*, vol. 12, no. 6, pp. 1678–1687, 2006.

[35] I. A. Marques, "Moduladores de Eletro-Absorção Integrados com Materiais Bidimensionais," Ph.D. dissertation, 2018.

[36] L. N. Binh, *Optical Modulation*, 1st ed. CRC Press, 2017.

[37] C. T. Phare, Y.-H. Daniel Lee, J. Cardenas, and M. Lipson, "Graphene electro-optic modulator with 30 GHz bandwidth," *Nature Photonics*, vol. 9, no. 8, pp. 511–514, 2015.

[38] M. Midrio, S. Boscolo, M. Moresco, M. Romagnoli, C. De Angelis, A. Locatelli, and A.-D. Capobianco, "Graphene–assisted critically–coupled optical ring modulator," *Optics Express*, vol. 20, no. 21, p. 23144, 2012.

[39] C. Qiu, W. Gao, R. Vajtai, P. M. Ajayan, J. Kono, and Q. Xu, "Efficient modulation of 1.55 μm radiation with gated graphene on a silicon microring resonator,"

Nano Letters, vol. 14, no. 12, pp. 6811–6815, 2014.

[40] W. Bogaerts, P. de Heyn, T. van Vaerenbergh, K. de Vos, S. Kumar Selvaraja, T. Claes, P. Dumon, P. Bienstman, D. van Thourhout, and R. Baets, "Silicon microring resonators," *Laser and Photonics Reviews*, vol. 6, no. 1, pp. 47–73, 2012.

[41] F. Zhou and C. Liang, "The absorption ring modulator based on few-layer graphene," *Journal of Optics*, vol. 21, no. 4, p. 045801, 2019.

[42] Z. Li, L. Bai, X. Li, E. Gu, L. Niu, and X. Zhang, "U-shaped micro-ring graphene electro-optic modulator," *Optics Communications*, vol. 428, pp. 200–205, 2018.

[43] Q. Xu, B. Schmidt, S. Pradhan, and M. Lipson, "Micrometre-scale silicon electro-optic modulator," *Nature*, vol. 435, no. 7040, pp. 325–327, 2005.

[44] X. Qiu, X. Ruan, Y. Li, and F. Zhang, "Multi-layer MOS capacitor based polarization insensitive electro-optic intensity modulator," *Optics Express*, vol. 26, no. 11, p. 13902, 2018.

[45] Y. Chenran, S. Khan, Z. R. Li, E. Simsek, and V. J. Sorger, "λ-Size ITO and Graphene-Based Electro-Optic Modulators on SOI," *IEEE Journal of Selected Topics in Quantum Electronics*, vol. 20, no. 4, pp. 40–49, 2014.

[46] Z. Ma, Z. Li, K. Liu, C. Ye, and V. J. Sorger, "Indium-Tin-Oxide for High-performance Electro-optic Modulation," *Nanophotonics*, vol. 4, no. 1, pp. 198–213, 2015.

[47] A. P. Vasudev, J.-H. Kang, J. Park, X. Liu, and M. L. Brongersma, "Electro-optical modulation of a silicon waveguide with an 'epsilon-near-zero' material," *Optics Express*, vol. 21, no. 22, p. 26387, 2013.

[48] K. S. Novoselov, A. K. Geim, S. V. Morozov, D. Jiang, Y. Zhang, S. V. Dubonos, I. V. Grigorieva, and A. A. Firsov, "Electric Field Effect in Atomically Thin Carbon Films," *Science*, vol. 306, no. 1, pp. 666–669, 2004.

[49] K. S. Novoselov, S. V. Morozov, T. M. G. Mohinddin, L. A. Ponomarenko, D. C. Elias, R. Yang, I. I. Barbolina, P. Blake, T. J. Booth, D. Jiang, J. Giesbers, E. W. Hill, and A. K. Geim, "Electronic properties of graphene," *physica status solidi (b)*, vol. 244, pp. 4106–4111, 2007.

[50] A. K. Geim and K. S. Novoselov, "The rise of graphene," *Nanoscience and Technology: a collection of reviews from nature journals*, pp. 11–19, 2009.

[51] K. S. Novoselov, V. I. Falko, L. Colombo, P. R. Gellert, M. G. Schwab, and K. Kim, "A roadmap for graphene," *Nature*, vol. 490, no. 7419, pp. 192–200, 2012.

[52] R. Murali, *Graphene Nanoelectronics*, 1st ed. Springer US, 2012.

[53] D. Johnson, "Graphene Paves the Way for Next Generation Plasmonics," *Comsol Multiphysics*, pp. 14–17, 2015.

[54] Q. Bao, H. H. Hoh, and Y. Zhang, *Graphene Photonics, Optoelectronics, and Plasmonics*, 1st ed. Pan Stanford Publishing, 2017.

[55] L. Britnell, R. M. Ribeiro, A. Eckmann, R. Jalil, B. D. Belle, A. Mishchenko, Y. J. Kim, R. V. Gorbachev, T. Georgiou, S. V. Morozov, A. N. Grigorenko, A. K. Geim, C. Casiraghi, A. H. C. Neto, and K. S. Novoselov, "Strong Light-Matter Interactions in Heterostructures of Atomically Thin Films," *Science*, vol. 340, no. 6138, pp. 1311–1314, 2013.

[56] K. S. Novoselov, A. K. Geim, S. V. Morozov, D. Jiang, M. I. Katsnelson, I. V. Grigorieva, S. V. Dubonos, and A. A. Firsov, "Two-dimensional gas of massless Dirac fermions in graphene," *Nature*, vol. 438, no. 7065, pp. 197–200, 2005.

[57] J. Wang, J. Song, X. Mu, and M. Sun, "Optoelectronic and photoelectric properties and applications of graphene-based nanostructures," *Materials Today Physics*, vol. 13, p. 100196, 2020.

[58] A. H. C. Neto, F. Guinea, N. M. R. Peres, K. S. Novoselov, and A. K. Geim, "The electronic properties of graphene," *Reviews of Modern Physics*, vol. 81, no. 1, pp. 109–162, 2007.

[59] R. R. Nair, P. Blake, A. N. Grigorenko, K. S. Novoselov, T. J. Booth, T. Stauber, N. M. R. Peres, and A. K. Geim, "Fine Structure Constant Defines Visual Transparency of Graphene," *Science*, vol. 320, no. 5881, p. 1308, 2008.

[60] J. Yan, Y. Zhang, P. Kim, and A. Pinczuk, "Electric Field Effect Tuning of Electron-Phonon Coupling in Graphene," *Physical Review Letters*, vol. 98, no. 16, p. 166802, 2007.

[61] K. Kim, J. Y. Choi, T. Kim, S. H. Cho, and H. J. Chung, "A role for graphene in silicon-based semiconductor devices," *Nature*, vol. 479, no. 7373, pp. 338–344, 2011.

[62] Z. Lu and W. Zhao, "Nanoscale electro-optic modulators based on graphene-slot waveguides," *Journal of the Optical Society of America B*, vol. 29, no. 6, p. 1490, 2012.

[63] F. Bonaccorso, Z. Sun, T. Hasan, and A. C. Ferrari, "Graphene photonics and optoelectronics," *Nature Photonics*, vol. 4, no. 9, pp. 611–622, 2010.

[64] X. Liu, K. Zang, J. H. Kang, J. Park, J. S. Harris, P. G. Kik, and M. L. Brongersma, "Epsilon-Near-Zero Si Slot-Waveguide Modulator," *ACS Photonics*, vol. 5, no. 11,

pp. 4484–4490, 2018.

[65] B. Sensale-Rodriguez, "Graphene-Based Optoelectronics," *Journal of Lightwave Technology*, vol. 33, no. 5, pp. 1100–1108, 2015.

[66] A. N. Grigorenko, M. Polini, and K. S. Novoselov, "Graphene plasmonics," *Nature Photonics*, vol. 6, no. 11, pp. 749–758, 2012.

[67] S. Qu, C. Ma, and H. Liu, "Tunable graphene-based hybrid plasmonic modulators for subwavelength confinement," *Scientific Reports*, vol. 7, no. 1, p. 5190, 2017.

[68] P. A. D. Gonçalves and N. M. Peres, *An Introduction to Graphene Plasmonics*, 1st ed. World Scientific, 2016.

[69] S. Luo, Y. Wang, X. Tong, and Z. Wang, "Graphene-based optical modulators," *Nanoscale Research Letters*, vol. 10, no. 1, p. 199, 2015.

[70] M. Liu, X. Yin, E. Ulin-Avila, B. Geng, T. Zentgraf, L. Ju, F. Wang, and X. Zhang, "A graphene-based broadband optical modulator," *Nature*, vol. 474, no. 7349, pp. 64–67, 2011.

[71] M. Liu, X. Yin, and X. Zhang, "Double-Layer Graphene Optical Modulator," *Nano Letters*, vol. 12, no. 3, pp. 1482–1485, 2012.

[72] C. Zhong, J. Li, and H. Lin, "Graphene-based all-optical modulators," *Frontiers of Optoelectronics*, vol. 13, no. 2, pp. 114–128, 2020.

[73] H. W. Shu, M. Jin, Y. S. Tao, and X. J. Wang, "Graphene-based silicon modulators," *Frontiers of Information Technology & Electronic Engineering*, vol. 20, no. 4, pp. 458–471, 2019.

[74] V. Sorianello, G. Contestabile, and M. Romagnoli, "Graphene on Silicon Modulators," *Journal of Lightwave Technology*, vol. 38, no. 10, pp. 2782–2789, 2020.

[75] J. Liu, Z. U. Khan, C. Wang, H. Zhang, and S. Sarjoghian, "Review of graphene modulators from the low to the high figure of merits," *Journal of Physics D: Applied Physics*, vol. 53, no. 23, p. 233002, 2020.

[76] M. Mohsin, D. Schall, M. Otto, A. Noculak, D. Neumaier, and H. Kurz, "Graphene based low insertion loss electro-absorption modulator on SOI waveguide," *Optics Express*, vol. 22, no. 12, p. 15292, 2014.

[77] A. Phatak, Z. Cheng, C. Qin, and K. Goda, "Design of electro-optic modulators based on graphene-on-silicon slot waveguides," *Optics Letters*, vol. 41, no. 11, p. 2501, 2016.

[78] Y. Hu, M. Pantouvaki, J. Van Campenhout, S. Brems, I. Asselberghs, C. Huyghe-

baert, P. Absil, and D. Van Thourhout, "Broadband 10 Gb/s operation of graphene electro-absorption modulator on silicon," *Laser & Photonics Reviews*, vol. 10, no. 2, pp. 307–316, 2016.

[79] C. Alessandri, I. Asselberghs, Y. Ban, S. Brems, C. Huyghebaert, J. Van Campe nhout, D. Van Thourhout, and M. Pantouvaki, "Broadband 20 Gbit/s Graphene-Si Electro-Absorption Modulator," in *2018 European Conference on Optical Communication (ECOC)*, no. 1. IEEE, 2018, pp. 1–3.

[80] M. Fan, H. Yang, P. Zheng, G. Hu, B. Yun, and Y. Cui, "Multilayer graphene electro-absorption optical modulator based on double-stripe silicon nitride waveguide," *Optics Express*, vol. 25, no. 18, p. 21619, 2017.

[81] M. K. Shah, S. W. Ye, X. H. Zou, F. Yuan, A. Jha, Y. L. Zhang, R. G. Lu, and Y. Liu, "Graphene-Assisted Electroabsorption Optical Modulator Using D-Microfiber," *IEEE Journal of Selected Topics in Quantum Electronics*, vol. 23, no. 1, pp. 89–93, 2017.

[82] V. Sorianello, M. Midrio, G. Contestabile, I. Asselberghs, J. Van Campenhout, C. Huyghebaert, I. Goykhman, A. K. Ott, A. C. Ferrari, and M. Romagnoli, "Graphene–silicon phase modulators with gigahertz bandwidth," *Nature Photonics*, vol. 12, no. 1, pp. 40–44, 2018.

[83] L. Ji, Y. Gao, Y. Xu, X. Sun, C. Wu, Y. Wu, and D. Zhang, "High figure of merit electro-optic modulator based on graphene on silicon dual-slot waveguide," *IEEE Journal of Quantum Electronics*, vol. 54, no. 6, pp. 1–7, 2018.

[84] Z. Yang, R. Lu, S. Cai, Y. Wang, Y. Zhang, X. Wang, and Y. Liu, "A CMOS-compatible and polarization-insensitive graphene optical modulator," *Optics Communications*, vol. 450, no. April, pp. 130–135, 2019.

[85] J. Luan, M. Fan, P. Zheng, H. Yang, G. Hu, B. Yun, and Y. Cui, "Design and Optimization of a Graphene Modulator Based on Hybrid Plasmonic Waveguide with Double Low-Index Slots," *Plasmonics*, vol. 14, no. 1, pp. 133–138, 2019.

[86] Y. Ma, J. Li, Z. Han, H. Maeda, and J. Pistora, "All-Dielectric Graphene-induced T-Slot Waveguide Electro-Optic Modulator With Polarization-Independent Operation," *IEEE Journal of Selected Topics in Quantum Electronics*, vol. 27, no. 3, pp. 1–8, 2021.

[87] W. Chen, X. Fan, P. Li, Y. Gao, L. Ji, X. Sun, and D. Zhang, "Polarization-Insensitive Electro-Absorption Modulator Based on Graphene-Silicon Nitride Hybrid Waveguide," *IEEE Photonics Journal*, vol. 13, no. 3, pp. 1–13, 2021.

[88] X. Zou, Y. Zhang, Z. Li, Y. Yang, S. Zhang, Z. Zhang, Y. Zhang, and Y. Liu,

"Polarization-Insensitive Phase Modulators Based on an Embedded Silicon-Graphene-Silicon Waveguide," *Applied Sciences*, vol. 9, no. 3, p. 429, 2019.

[89] Z. Ma, M. H. Tahersima, S. Khan, and V. J. Sorger, "Two-Dimensional Material-Based Mode Confinement Engineering in Electro-Optic Modulators," *IEEE Journal of Selected Topics in Quantum Electronics*, vol. 23, no. 1, pp. 81–88, 2017.

[90] X. Hu and J. Wang, "Design of graphene-based polarization-insensitive optical modulator," *Nanophotonics*, vol. 7, no. 3, pp. 651–658, 2018.

[91] Y. Meng, S. Ye, Y. Shen, Q. Xiao, X. Fu, R. Lu, Y. Liu, and M. Gong, "Waveguide Engineering of Graphene Optoelectronics—Modulators and Polarizers," *IEEE Photonics Journal*, vol. 10, no. 1, pp. 1–17, 2018.

[92] R. Hao, W. Du, E. P. Li, and H. S. Chen, "Graphene Assisted TE/TM-Independent Polarizer Based on Mach–Zehnder Interferometer," *IEEE Photonics Technology Letters*, vol. 27, no. 10, pp. 1112–1115, 2015.

[93] X. Hu, C. Gui, and J. Wang, "A Graphene-based Polarization-Insensitive Optical Modulator," in *Advanced Photonics for Communications*, vol. 2. OSA, 2014.

[94] S. W. Ye, D. Liang, R. G. Lu, M. K. Shah, X. H. Zou, F. Yuan, F. Yang, and Y. Liu, "Polarization-Independent Modulator by Partly Tilted Graphene-Induced Electro-Absorption Effect," *IEEE Photonics Technology Letters*, vol. 29, no. 1, pp. 23–26, 2017.

[95] M. K. Shah, R. G. Lu, T. L. Liu, and Y. Liu, "Polarization-insensitive electro-absorption optical modulator using ITO-enhanced D-fiber," *International Topical Meeting on Microwave Photonics (MWP)*, vol. 1, pp. 1–4, 2017.

[96] Y. Xu, F. Li, Z. Kang, D. Huang, X. Zhang, H. Y. Tam, and P. K. Wai, "Hybrid graphene-silicon based polarization-insensitive electro-absorption modulator with high-modulation efficiency and ultra-broad bandwidth," *Nanomaterials*, vol. 9, no. 2, pp. 1–15, 2019.

[97] R. Hao, W. Du, H. Chen, X. Jin, L. Yang, and E. Li, "Ultra-compact optical modulator by graphene induced electro-refraction effect," *Applied Physics Letters*, vol. 103, no. 6, p. 061116, 2013.

[98] X. Peng, E. Li, and R. Hao, "Graphene-aluminum oxide metamaterial for a compact polarization-independent modulator," in *2015 IEEE MTT-S International Microwave Workshop Series on Advanced Materials and Processes for RF and THz Applications (IMWS-AMP)*. IEEE, 2015, pp. 1–3.

[99] S. Ye, Z. Wang, L. Tang, Y. Zhang, R. Lu, and Y. Liu, "Electro-absorption optical

modulator using dual-graphene-on-graphene configuration," *Optics Express*, vol. 22, no. 21, p. 26173, 2014.

[100] A. Yariv and P. Yeh, *Photonics - Optical Electronics in Modern Communications*, 6th ed. Oxford University Press, 2007.

[101] S. Kasap, *Optoelectronics and Photonics: Principles and Practices*, 2nd ed. Pearson Education Limited, 2013.

[102] D. S. Chemla, T. C. Damen, D. A. B. Miller, A. C. Gossard, and W. Wiegmann, "Electroabsorption by Stark effect on room-temperature excitons in GaAs/GaAlAs multiple quantum well structures," *Applied Physics Letters*, vol. 42, no. 10, pp. 864–866, 1983.

[103] T. Kawanishi, *Electro-optic Modulation for Photonic Networks*, 1st ed. Springer International Publishing, 2022.

[104] Y. H. Kuo, Y. K. Lee, Y. Ge, S. Ren, J. E. Roth, T. I. Kamins, D. A. B. Miller, and J. S. Harris, "Strong quantum-confined Stark effect in germanium quantum-well structures on silicon," *Nature*, vol. 437, no. 7063, pp. 1334–1336, 2005.

[105] J. H. Chen, C. Jang, S. Xiao, M. Ishigami, and M. S. Fuhrer, "Intrinsic and extrinsic performance limits of graphene devices on SiO2," *Nature Nanotechnology*, vol. 3, no. 4, pp. 206–209, 2008.

[106] C. S. Li and F. Tong, "Crosstalk and interference penalty in all-optical networks using static wavelength routers," *Journal of Lightwave Technology*, vol. 14, no. 6, pp. 1120–1126, 1996.

[107] G. P. Agrawal, *Sistemas de Comunicações Ópticas*, 4th ed. Elsevier Editora Ltda., 2014.

[108] B. Mukherjee, *Optical WDM Networks*, 1st ed. Springer, 2006.

[109] "iXblue Photonics - NNIR-MX-LN-40." 2022, Accessed in 2022-05-05. [Online]. Available: https://www.ixblue.com/wp-content/uploads/2022/01/NIR-MX-LN-40_1.pdf

[110] "ThorLabs LiNbO3 MZM Modulators," 2022, Accessed in 2022-05-05. [Online]. Available: https://www.thorlabs.com/newgrouppage9.cfm?objectgroup_id=3918

[111] "Fujitsu 40Gbs NRZ LiNbO3 External Modulator." 2022, Accessed in 2022-05-05. [Online]. Available: https://www.fujitsu.com/downloads/OPTCMP/lineup/40gln/40Glnnrz-catalog.pdf

[112] M. Dragoman and D. Dragoman, *2D Nanoelectronics*, 1st ed. Springer International Publishing, 2017.

[113] H. Raza, *Graphene Nanoelectronics*, 1st ed. Springer, 2012.

[114] A. K. Geim and I. V. Grigorieva, "Van der Waals heterostructures," *Nature*, vol. 499, no. 7459, pp. 419–425, 2013.

[115] S. Nazarpour and S. R. Waite, *Graphene Technology*, 1st ed. Wiley-VCH Verlag GmbH & Co. KGaA, 2016.

[116] C. Lee, X. Wei, J. W. Kysar, and J. Hone, "Measurement of the Elastic Properties and Intrinsic Strength of Monolayer Graphene," *Science*, vol. 321, no. 5887, pp. 385–388, 2008.

[117] M. Rapisarda, G.-P. Malfense Fierro, and M. Meo, "Ultralight graphene oxide/polyvinyl alcohol aerogel for broadband and tuneable acoustic properties," *Scientific Reports*, vol. 11, no. 1, p. 10572, 2021.

[118] S. Yan, X. Zhu, L. H. Frandsen, S. Xiao, N. A. Mortensen, J. Dong, and Y. Ding, "Slow-light-enhanced energy efficiency for graphene microheaters on silicon photonic crystal waveguides," *Nature Communications*, vol. 8, no. 1, p. 14411, 2017.

[119] A. A. Balandin, S. Ghosh, W. Bao, I. Calizo, D. Teweldebrhan, F. Miao, and C. N. Lau, "Superior Thermal Conductivity of Single-Layer Graphene," *Nano Letters*, vol. 8, no. 3, pp. 902–907, 2008.

[120] Z. Sun, T. Hasan, F. Torrisi, D. Popa, G. Privitera, F. Wang, F. Bonaccorso, D. M. Basko, and A. C. Ferrari, "Graphene Mode-Locked Ultrafast Laser," *ACS Nano*, vol. 4, no. 2, pp. 803–810, 2010.

[121] I. Llatser, C. Kremers, A. Cabellos-Aparicio, J. M. Jornet, E. Alarcón, and D. N. Chigrin, "Graphene-based nano-patch antenna for terahertz radiation," *Photonics and Nanostructures - Fundamentals and Applications*, vol. 10, no. 4, pp. 353–358, 2012.

[122] C. H. Liu, Y. C. Chang, T. B. Norris, and Z. Zhong, "Graphene photodetectors with ultra-broadband and high responsivity at room temperature," *Nature Nanotechnology*, vol. 9, no. 4, pp. 273–278, 2014.

[123] S. J. Han, A. V. Garcia, S. Oida, K. A. Jenkins, and W. Haensch, "Graphene radio frequency receiver integrated circuit," *Nature Communications*, vol. 5, no. 1, p. 3086, 2014.

[124] Z. Q. Li, E. A. Henriksen, Z. Jiang, Z. Hao, M. C. Martin, P. Kim, H. L. Stormer, and D. N. Basov, "Dirac charge dynamics in graphene by infrared spectroscopy," *Nature Physics*, vol. 4, no. 7, pp. 532–535, 2008.

[125] V. K. Sadaghiani, M. Zavvari, M. B. Tavakkoli, and A. Horri, "Design of

graphene-based hybrid waveguides for nonlinear applications," *Optical and Quantum Electronics*, vol. 51, no. 2, p. 49, 2019.

[126] M. Houssa, A. Dimoulas, and A. Molle, *2D Materials for Nanoelectronics*, 1st ed. CRC Press, 2016.

[127] M. Sharon and M. Sharon, *Graphene - An introduction to the Fundamentals and Industrial Applications*, 1st ed. Scrivener Publishing LLC., 2015.

[128] R. Spickermann, M. Peters, and N. Dagli, "A polarization independent GaAs-AlGaAs electrooptic modulator," *IEEE Journal of Quantum Electronics*, vol. 32, no. 5, pp. 764–769, 1996.

[129] K. Bolotin, K. Sikes, Z. Jiang, M. Klima, G. Fudenberg, J. Hone, P. Kim, and H. Stormer, "Ultrahigh electron mobility in suspended graphene," *Solid State Communications*, vol. 146, no. 9-10, pp. 351–355, 2008.

[130] L. Ren, Q. Zhang, J. Yao, Z. Sun, R. Kaneko, Z. Yan, S. Nanot, Z. Jin, I. Kawayama, M. Tonouchi, J. M. Tour, and J. Kono, "Terahertz and Infrared Spectroscopy of Gated Large-Area Graphene," *Nano Letters*, vol. 12, no. 7, pp. 3711–3715, 2012.

[131] B. Sensale-Rodriguez, R. Yan, M. M. Kelly, T. Fang, K. Tahy, W. S. Hwang, D. Jena, L. Liu, and H. G. Xing, "Broadband graphene terahertz modulators enabled by intraband transitions," *Nature Communications*, vol. 3, no. 1, pp. 780–787, 2012.

[132] B. Sensale-Rodriguez, R. Yan, M. Zhu, D. Jena, L. Liu, and H. Grace Xing, "Efficient terahertz electro-absorption modulation employing graphene plasmonic structures," *Applied Physics Letters*, vol. 101, no. 26, p. 261115, 2012.

[133] N. Youngblood, Y. Anugrah, R. Ma, S. J. Koester, and M. Li, "Multifunctional Graphene Optical Modulator and Photodetector Integrated on Silicon Waveguides," *Nano Letters*, vol. 14, no. 5, pp. 2741–2746, 2014.

[134] M. Mohsin, D. Neumaier, D. Schall, M. Otto, C. Matheisen, A. Lena Giesecke, A. A. Sagade, and H. Kurz, "Experimental verification of electro-refractive phase modulation in graphene," *Scientific Reports*, vol. 5, no. 1, p. 10967, 2015.

[135] I. Chakraborty, K. Debnath, and V. Dixit, "Low-energy high-speed graphene modulator for on-chip communication," *OSA Continuum*, vol. 2, no. 4, p. 1273, 2019.

[136] D. Miller, "Device Requirements for Optical Interconnects to Silicon Chips," *Proceedings of the IEEE*, vol. 97, no. 7, pp. 1166–1185, 2009.

[137] S. J. Koester and M. Li, "High-speed waveguide-coupled graphene-on-graphene

optical modulators," *Applied Physics Letters*, vol. 100, no. 17, p. 171107, 2012.

[138] S. Y. Zhou, G. H. Gweon, J. Graf, A. V. Fedorov, C. D. Spataru, R. D. Diehl, Y. Kopelevich, D. H. Lee, S. G. Louie, and A. Lanzara, "First direct observation of Dirac fermions in graphite," *Nature Physics*, vol. 2, no. 9, pp. 595–599, 2006.

[139] M. Aliofkhazraei, N. Ali, W. I. Milne, C. S. Ozkan, S. Mitura, and J. L. Gervasoni, *Graphene Science Handbook*, 1st ed. CRC Press, 2016.

[140] R. Amin, Z. Ma, R. Maiti, S. Khan, J. B. Khurgin, H. Dalir, and V. J. Sorger, "Attojoule-efficient graphene optical modulators," *Applied Optics*, vol. 57, no. 18, pp. D130–D140, 2018.

[141] R. E. P. de Oliveira and C. J. S. de Matos, "Graphene Based Waveguide Polarizers: In-Depth Physical Analysis and Relevant Parameters," *Scientific Reports*, vol. 5, no. 1, pp. 1–8, 2015.

[142] M. S. Kwon, "Discussion of the Epsilon-Near-Zero Effect of Graphene in a Horizontal Slot Waveguide," *IEEE Photonics Journal*, vol. 6, no. 3, pp. 1–9, 2014.

[143] C. H. Park, L. Yang, Y. W. Son, M. L. Cohen, and S. G. Louie, "Anisotropic behaviours of massless Dirac fermions in graphene under periodic potentials," *Nature Physics*, vol. 4, no. 3, pp. 213–217, 2008.

[144] Z. Chang and K. S. Chiang, "Experimental verification of optical models of graphene with multimode slab waveguides," *Optics Letters*, vol. 41, no. 9, p. 2129, 2016.

[145] J. E. Proctor, D. A. M. Armada, and A. Vijayaraghavan, *An Introduction to Graphene and Carbon Nanotubes*, 1st ed. CRC Press, 2016.

[146] A. Vakil and N. Engheta, "Transformation Optics Using Graphene," *Science*, vol. 332, no. 6035, pp. 1291–1294, 2011.

[147] X. Hu and J. Wang, "High Figure of Merit Graphene Modulator Based on Long-Range Hybrid Plasmonic Slot Waveguide," *IEEE Journal of Quantum Electronics*, vol. 53, no. 3, pp. 1–8, 2017.

[148] J. Gosciniak, D. T. H. Tan, and B. Corbett, "Enhanced performance of graphene-based electro-absorption waveguide modulators by engineered optical modes," *Journal of Physics D: Applied Physics*, vol. 48, no. 23, p. 235101, 2015.

[149] W. Gao, J. Shu, C. Qiu, and Q. Xu, "Excitation of Plasmonic Waves in Graphene by Guided-Mode Resonances," *ACS Nano*, vol. 6, no. 9, pp. 7806–7813, 2012.

[150] M. Najafi Hajivar and M. Hosseini Farzad, "Broadband polarization-insensitive

amplitude and phase modulators based on graphene-covered buried and ridge silicon waveguides," *Optics Communications*, vol. 472, no. 125860, p. 13, 2020.

[151] A. A. Sayem, M. R. Mahdy, I. Jahangir, and M. S. Rahman, "Ultrathin ultra-broadband electro-absorption modulator based on few-layer graphene based anisotropic metamaterial," *Optics Communications*, vol. 384, no. 1, pp. 50–58, 2017.

[152] J. Gosciniak and D. T. H. Tan, "Theoretical investigation of graphene-based photonic modulators," *Scientific Reports*, vol. 3, no. 1, p. 1897, 2013.

[153] G. W. Hanson, "Dyadic Green's functions and guided surface waves for a surface conductivity model of graphene," *Journal of Applied Physics*, vol. 103, no. 6, p. 064302, 2008.

[154] T. Stauber, N. M. R. Peres, and A. K. Geim, "The optical conductivity of graphene in the visible region of the spectrum," *Physical Review B*, vol. 78, no. 8, p. 085432, 2008.

[155] F. Jabbarzadeh, M. Heydari, and A. Habibzadeh-Sharif, "A comparative analysis of the accuracy of Kubo formulations for graphene plasmonics," *Materials Research Express*, vol. 6, no. 8, p. 086209, 2019.

[156] C. Hwang, D. A. Siegel, S.-K. Mo, W. Regan, A. Ismach, Y. Zhang, A. Zettl, and A. Lanzara, "Fermi velocity engineering in graphene by substrate modification," *Scientific Reports*, vol. 2, no. 1, p. 590, 2012.

[157] F. Wang, Y. Zhang, C. Tian, C. Girit, A. Zettl, M. Crommie, and Y. R. Shen, "Gate-variable optical transitions in graphene," *Science*, vol. 320, no. 5873, pp. 206–209, 2008.

[158] S. Balci and C. Kocabas, *Graphene Photonics, Optoelectronics, and Plasmonics*. Jenny Stanford Publishing, 2017.

[159] S. Mishra and D. P. Hansora, *Graphene Nanomaterials*, 1st ed. Pan Stanford Publishing Pte. Ltd., 2018.

[160] M. Romagnoli, V. Sorianello, M. Midrio, F. H. L. Koppens, C. Huyghebaert, D. Neumaier, P. Galli, W. Templ, A. D'Errico, and A. C. Ferrari, "Graphene-based integrated photonics for next-generation datacom and telecom," *Nature Reviews Materials*, vol. 3, no. 10, pp. 392–414, 2018.

[161] M. Seimetz, *High-Order Modulation for Optical Fiber Transmission*, 1st ed. Springer, 2009.

[162] Y. Zhou, R. Lu, G. Wang, J. Lyu, M. Tan, L. Shen, R. Lin, Z. Yang, and Y. Liu, "Graphene-Based Polarization-Independent Mid-Infrared Electro-Absorption

Modulator Integrated in a Chalcogenide Glass Waveguide," *Nanoscale Research Letters*, vol. 16, no. 1, p. 80, 2021.

[163] M. K. Shah, R. Lu, D. Peng, Y. Ma, S. Ye, Y. Zhang, Z. Zhang, and Y. Liu, "Graphene-Assisted Polarization-Insensitive Electro-absorption Optical Modulator," *IEEE Transactions on Nanotechnology*, vol. 16, no. 6, pp. 1004–1010, 2017.

[164] S. Sayan, S. Aravamudhan, B. W. Busch, W. H. Schulte, F. Cosandey, G. D. Wilk, T. Gustafsson, and E. Garfunkel, "Chemical vapor deposition of HfO_2 films on Si(100)," *Journal of Vacuum Science & Technology A: Vacuum, Surfaces, and Films*, vol. 20, no. 2, pp. 507–512, 2002.

[165] M. Al-Kuhaili, "Optical properties of hafnium oxide thin films and their application in energy-efficient windows," *Optical Materials*, vol. 27, no. 3, pp. 383–387, 2004.

[166] Y. Chen, "Nanofabrication by electron beam lithography and its applications: A review," *Microelectronic Engineering*, vol. 135, pp. 57–72, 2015.

[167] A. Pimpin and W. Srituravanich, "Reviews on micro- and nanolithography techniques and their applications," *Engineering Journal*, vol. 16, no. 1, pp. 37–55, 2012.

[168] S. Cabrini and S. Kawata, *Nanofabrication Handbook*, 1st ed. CRC Press, 2012.

[169] I. H. Malitson, "Interspecimen Comparison of the Refractive Index of Fused Silica," *Journal of the Optical Society of America*, vol. 55, no. 10, p. 1205, 1965.

[170] M. Kleinert, F. Herziger, P. Reinke, C. Zawadzki, D. de Felipe, W. Brinker, H.-G. Bach, N. Keil, J. Maultzsch, and M. Schell, "Graphene-based electro-absorption modulator integrated in a passive polymer waveguide platform," *Optical Materials Express*, vol. 6, no. 6, p. 1800, 2016.

[171] H. Agarwal, B. Terrés, L. Orsini, A. Montanaro, V. Sorianello, M. Pantouvaki, K. Watanabe, T. Taniguchi, D. V. Thourhout, M. Romagnoli, and F. H. L. Koppens, "2D-3D integration of hexagonal boron nitride and a high-κ dielectric for ultrafast graphene-based electro-absorption modulators," *Nature Communications*, vol. 12, no. 1, p. 1070, 2021.

[172] S. W. Ye, F. Yuan, X. H. Zou, M. K. Shah, R. G. Lu, and Y. Liu, "High-speed optical phase modulator based on graphene-silicon waveguide," *IEEE Journal on Selected Topics in Quantum Electronics*, vol. 23, no. 1, pp. 76–80, 2017.

[173] M. Midrio, P. Galli, M. Romagnoli, L. C. Kimerling, and J. Michel, "Graphene-

based optical phase modulation of waveguide transverse electric modes," *Photonics Research*, vol. 2, no. 3, p. A34, 2014.

[174] M. Haruna and J. Koyama, "Thermo-optic effect in $LiNbO_3$, for light deflection and switching," *Electronics Letters*, vol. 17, no. 22, p. 842, 1981.

[175] A. K. Dutta, N. K. Dutta, M. Fujiwara, and H. Kogelnik, *WDM Technologies*. Elsevier Academic Press, 2004, vol. 3.

[176] K. M. Sivalingam and S. Subramaniam, *Optical WDM Networks - Principles and Practice*, 1st ed. Kluwer Academic Publishers, 2002.

[177] S. Zhang, Z. Li, and F. Xing, "Review of Polarization Optical Devices Based on Graphene Materials." *International journal of molecular sciences*, vol. 21, no. 5, p. 1608, 2020.

[178] X. Hu, Y. Zhang, D. Chen, X. Xiao, and S. Yu, "Design and Modeling of High Efficiency Graphene Intensity/Phase Modulator Based on Ultra-Thin Silicon Strip Waveguide," *Journal of Lightwave Technology*, vol. 37, no. 10, pp. 2284–2292, 2019.

[179] R. Ghosh, P. Bhardwaj, S. Subramanian, M. Jaiswal, and A. Dhawan, "Design of electro-optic modulators and switches based on graphene and phase change materials," *Integrated Optics: Design, Devices, Systems, and Applications V*, no. April, p. 52, 2019.

[180] Y. Shen, N. C. Harris, S. Skirlo, M. Prabhu, T. Baehr-Jones, M. Hochberg, X. Sun, S. Zhao, H. Larochelle, D. Englund, and M. Soljačić, "Deep learning with coherent nanophotonic circuits," *Nature Photonics*, vol. 11, no. 7, pp. 441–446, 2017.

[181] M. Asghari and A. V. Krishnamoorthy, "Energy-Efficient Communication," *Nature Photonics*, vol. 5, pp. 268–270, 2011.

[182] H. Li, Y. Anugrah, S. J. Koester, and M. Li, "Optical absorption in graphene integrated on silicon waveguides," *Applied Physics Letters*, vol. 101, no. 11, p. 111110, 2012.

[183] H. Zhong, Z. Zhang, B. Chen, H. Xu, D. Yu, L. Huang, and L. Peng, "Realization of low contact resistance close to theoretical limit in graphene transistors," *Nano Research*, vol. 8, no. 5, pp. 1669–1679, 2015.

[184] F. Xia, V. Perebeinos, Y. M. Lin, Y. Wu, and P. Avouris, "The origins and limits of metal-graphene junction resistance." *Nature nanotechnology*, vol. 6, no. 3, pp. 179–84, 2011.

[185] S. De and J. N. Coleman, "Are There Fundamental Limitations on the Sheet

Resistance and Transmittance of Thin Graphene Films?" *ACS Nano*, vol. 4, no. 5, pp. 2713–2720, 2010.

[186] T. Salgals, I. Kurbatska, V. Bobrovs, and S. Spolitis, "Research of PAM-4 Modulated WDM-PON Architecture for 5G Millimeter-wave Hybrid Photonics-wireless Interface," in *2019 Photonics & Electromagnetics Research Symposium - Fall (PIERS - Fall)*, vol. 2. IEEE, 2019, pp. 728–734.

[187] S. Zhou, H. T. Wu, K. Sadeghipour, C. Scarcella, C. Eason, M. Rensing, M. J. Power, C. Antony, P. O'Brien, P. D. Townsend, and P. Ossieur, "Optimization of PAM-4 transmitters based on lumped silicon photonic MZMs for high-speed short-reach optical links," *Optics Express*, vol. 25, no. 4, p. 4312, 2017.

[188] M. Carvalho, E. A. Thoroh de Souza, and L. Saito, "Graphene-based PAM-4 modulator compatible with CMOS platform operating over DWDM C-Band," *Results in Optics*, vol. 5, p. 100110, 2021.

[189] I. A. Marques and R. E. P. de Oliveira, "Design of a DAC-less PAM-4 integrated optical modulator based on silicon photonics with graphene," in *2017 SBMO/IEEE MTT-S International Microwave and Optoelectronics Conference (IMOC)*, vol. 2017-Janua. IEEE, 2017, pp. 1–4.

[190] R. Li, D. Patel, A. Samani, E. El Fiky, Z. Xing, M. Morsy-Osman, and D. V. Plant, "Silicon Photonic Ring-Assisted MZI for 50 Gb/s DAC-Less and DSP-Free PAM-4 Transmission," *IEEE Photonics Technology Letters*, vol. 29, no. 12, pp. 1046–1049, 2017.

[191] D. Soma, Y. Wakayama, S. Beppu, S. Sumita, T. Tsuritani, T. Hayashi, T. Nagashima, M. Suzuki, M. Yoshida, K. Kasai, M. Nakazawa, H. Takahashi, K. Igarashi, I. Morita, and M. Suzuki, "10.16-Peta-bit/s Dense SDM/WDM Transmission over 6-Mode 19-Core Fiber across the C+L Band," *Journal of Lightwave Technology*, vol. 36, no. 6, pp. 1–1, 2018.

[192] A. Sano, T. Kobayashi, S. Yamanaka, A. Matsuura, H. Kawakami, Y. Miyamoto, K. Ishihara, and H. Masuda, "102.3-Tb/s (224 × 548-Gb/s) C- and Extended L-band All-Raman Transmission over 240 km Using PDM-64QAM Single Carrier FDM with Digital Pilot Tone," in *National Fiber Optic Engineers Conference*. OSA, 2012.

[193] K. Szczerba, P. Westbergh, J. Karout, J. S. Gustavsson, Haglund, M. Karlsson, P. A. Andrekson, E. Agrell, and A. Larsson, "4-PAM for High-Speed Short-Range Optical Communications," *Journal of Optical Communications and Networking*, vol. 4, no. 11, p. 885, 2012.

[194] X. Hu, Y. Long, M. Ji, A. Wang, L. Zhu, Z. Ruan, Y. Wang, and J. Wang, "Graphene-silicon microring resonator enhanced all-optical up and down wavelength conversion of QPSK signal," *Optics Express*, vol. 24, no. 7, p. 7168, 2016.

[195] J. Cui, G.-W. Lu, H. Wang, and Y. Ji, "On-Chip Optical Vector Quadrature De-Multiplexer Proposal for QAM De-Aggregation by Single Bi-Directional SOA-Based Phase-Sensitive Amplifier," *IEEE Access*, vol. 7, pp. 763–772, 2019.